Σ-Δ Modulators—Stability Analysis and Optimization

Lars Risbo
Electronics Institute, Bldg. 349,
Technical University of Denmark, DK-2800 Lyngby, Denmark
e-mail lrisbo@eiffel.ei.dth.dk

June 16, 1994

Contents

List of Figures

List of Tables

Preface

The present thesis has been submitted in partial fulfillment of the requirements for the Ph.D. degree at the Technical University of Denmark. The work has been carried out at the Electronics Institute Bldg. 349 during the period Nov. 1 1991 to April 31 1994.

My interest in the field of Σ-Δ modulation originates from the fall of 1990 where Compact Disc players with bitstream digital-to-analog converters became widespread. From the beginning of the era of the Compact Disc, the manufacturers were competing on higher and higher numbers of bits in claimed resolution, and suddenly a new type of converters were introduced using only a single bit.

I grew very fond of these new strange single-bit converters due to my background in the field of digital signal processing combined with my affection for music and systems for sound reproduction.

In february 1991, I started my masters project at the Electronics Institute. My topic was how to design stable high-order Σ-Δ modulators. The result of the project was a number of design tools and an approximate stability criterion based on quasilinear analysis. One of the chapters in this thesis includes extensions of the key results.

I received a scholarship from the Technical University of Denmark in november 1991, which enabled me to proceed with a Ph.D. study. My intention was partly to implement a Σ-Δ digital-to-analog converter with the best possible sound quality and partly to make further investigations on the stability problems concerned with Σ-Δ modulation.

I would like to thank a number of persons for their help and contributions. First of all, I would like to thank my advisors assoc. professors Peter K. Møller and John Aasted Sørensen for their never failing support and their efforts in making a pleasant and stimulating climate in the digital signal processing group. Peter A. Toft, Jan Larsen and Carsten Knudsen are thanked for a critical proof reading and review of the manuscript.

I am also very grateful for a number of persons with whom i have had enlightening discussions on the theoretical work: Robert Adams (Analog Devices USA), Truong-Thao Nguyen (Columbia Univ.), HongMo Wang (Bell Labs.), the “Junta” at the Electronics Institute (Jan Larsen, Peter A. Toft, Kim V. Hansen), Lars K. Hansen (EI) and Carsten Knudsen (MIDIT/CATS).

The practical implementation of the audio DAC was carried out in cooperation with Thomas Mørch (LIE) who contributed with a part of the printed circuit design. Jørgen Krogh (Analog Devices, Denmark) contributed with chip samples for evaluation in the DAC. Concerning the analog design, i received a lot of good advice from Peter Shah (EI/Imperial College, UK), Gudmundur Bogason (EI) and Michael Smedegaard Pedersen (LIE/Harman Marketing Europe).

Abstract

Σ-Δ modulation is widely used in high-performance data converters. The modulation process encodes a high-resolution discrete-time signal into a two-level (i.e, one-bit) signal with an increased sample rate. This provides speed to be traded for resolution. In the spectral domain, this effect is known as noise-shaping, i.e., the error of the one-bit signal is removed from a low-frequency band and concentrated at high frequencies.

A Σ-Δ modulator consists of a one-bit quantizer embedded in a feedback loop with a linear loop filter. Consequently, these modulators are highly nonlinear dynamical systems. For some types of loop filters, the modulators may be chaotic. One of the major drawbacks of Σ-Δ modulators is the potential risk of instability. This is especially the case for modulators with high-order loop filters. Instability is normally considered as the major problem of Σ-Δ modulator design.

The stability problem is pursued in this thesis. This is initially done from a nonlinear dynamics point of view. One of the conclusions is that chaotic modulators loose the stability due to a boundary crisis emerging when the attractor collides with the associated basin of attraction. The degree of instability is characterized by the so-called escape rate.

The stability is also investigated using *symbolic dynamics*. It is shown that the stability is closely related to the number of admissible limit cycles.

Some modulators are defined as being *unreliable*, i.e., the transition to the unstable regime is not a well defined point. Such modulators can be seemingly stable using simulations of moderate length. The instability will only appear in real-time implementations or very long simulations.

The thesis presents constrained optimization methods which are capable of finding reliable modulators with optimum signal-to-noise ratio. The method combines exact state-space analysis with approximate quasilinear modeling. The optimization tools have been used for the design of a 32 times oversampling 8th order Σ-Δ audio D/A-converter implemented using Field Programmable Gate Array (FPGA) circuits

Methods for suppression of the predominant tones near half the sample rate are investigated. The use of dithering and chaos are found to be equally efficient and equivalent in many respects. A new method for designing chaotic modulators is also introduced, i.e., the use of all-pass terms in the noise transfer function.

Finally, a new class of modulators using one-bit vector quantization is proposed. It is shown that the introduction of a vector quantizer can enhance the stability. Furthermore, the vector quantizer seems to reduce the amplitude of the tone near half the sample rate.

List of Symbols

n, k	Discrete time indices.
f_s	The sample rate.
$x(k)$	Modulator input signal.
$y(k)$	Modulator output signal.
$e(k)$	Quantizer input signal (error signal).
σ_e^2	Variance of $e(k)$.
$\mathcal{F}(\cdot)$	System map of a discrete-time dynamical sytem.
$\mathrm{D}\mathcal{F}(\cdot)$	Functional matrix (Jacobian) of $\mathcal{F}$.
$\mathcal{F}^{-1}(C)$	Denotes the preimage of the set C with respect to $\mathcal{F}$, i.e., the elements for which $\mathcal{F}(x) \in C$.
L	Limit set, defined in Definition 2.2.
B_L	Basin of attraction for the limit set L, defined in Definition 2.3.
∂B_L	Boundary of the basin of attraction for the limit set L.
$\boldsymbol{A}$	Transition matrix of a linear filter described in the state-space.
$\boldsymbol{x}_n$	State vector at time-step n.
S	The state-space of a modulator.
S_+	The part of the state-space for which a positive code is produced.
S_-	The part of the state-space for which a negative code is produced.
W	A bounding set which usually is supposed to surround a limit set.
U	The noninvertible region of a map $\mathcal{F}$ associated with a modulator.
V	The preimage of U.
$\Pr\{\cdot\}$	Probability.
γ	The escape rate, defined in As. 3.2.

$(\overline{p,k})$	A periodic output code sequence with period $p+k$ composed of p positive codes followed by k negative codes.
Λ	The expansion factor given as the product of the moduli of the system eigenvalues outside the unit circle, defined in Eq. (4.7).
$\|\cdot\|_1$	One-norm, i.e., sum of magnitudes.
$\|\cdot\|_\infty$	Infinity-norm, i.e., maximum magnitude.
$\|\cdot\|_2$	Two-norm, i.e., the square root of the sum of squares.
$H(z)$	Modulator feedback (loop) filter.
K	Linearized quantizer gain.
$q(k)$	Quantization noise of a quantizer.
σ_q^2	Variance of $q(k)$.
σ_b^2	Modulator output noise power within the base-band.
$\mathrm{NTF}(z)$	Noise Transfer Function from quantization noise source to modulator output, defined in Eq. (6.3). $\mathrm{ntf}(k)$ is the associated impulse response.
$\mathrm{STF}(z)$	Signal Transfer Function from modulator input to modulator output, defined in Eq. (6.2).
$\mathrm{ETF}(z)$	Error Transfer Function from quantization noise to quantizer input, defined in Eq. (6.26).
$\mathrm{A}(K)$	Noise amplification factor as a function of the quantizer gain, defined in Eq. (6.7)
A_{min}	Minimum of $\mathrm{A}(K)$.
$\mathrm{V}\{x\}$	Variance of x.
$\mathrm{Cov}\{x,y\}$	Covariance of x and y.
m_y	Mean value of the quantizer output $y(k)$.
pdf	Probability density function.
$\mathrm{S}(K)$	One-norm of $\mathrm{ntf}(k)$ versus the quantizer gain K, defined in Eq. (7.9).
S_{min}	Minimum of $\mathrm{S}(K)$.
MSA	Maximum Stable Amplitude. The maximal constant input amplitude for which a modulator is stable.

Chapter 1

Introduction

1.1 Oversampled One-bit Signal Encoding

When a signal is to be transmitted through a channel, a signal encoding scheme or a modulation is needed. The encoder accommodates the information of the signal into a form suitable for the channel. It is very common that the channel accepts a sequence of binary symbols, i.e., a one-bit signal.

A general signal transmission system using a one-bit channel is shown in Fig. 1.1. The signal source is in this case a discrete-time continuous amplitude signal which is low-pass filtered, i.e., the encoder input $x(n)$ is oversampled by the factor R= $\frac{f_s}{2f_c}$ where f_s is the sample rate and f_c is the filter cut-off frequency. The encoder transforms this oversampled signal into a one-bit signal ready for the channel. The decoder produces an estimate $\hat{x}(n)$ which approximates $x(k)$.

The performance of a signal transmission system can be assessed using a distortion measure such as the Mean Square Error (MSE), i.e., the mean value of $(x(n) - \hat{x}(n))^2$. It is also common to express the maximal signal-to-noise ratio (SNR), i.e., the maximum ratio between the signal power and the MSE. The SNR s typically measured for sinusoidal input.

In terms of information theory, the information capacity (rate) of the channel is one bit per sample. For a given signal source and information rate, the minimum attainable MSE is given by the so-called *Rate-Distortion* curve of the source [6]. The performance given

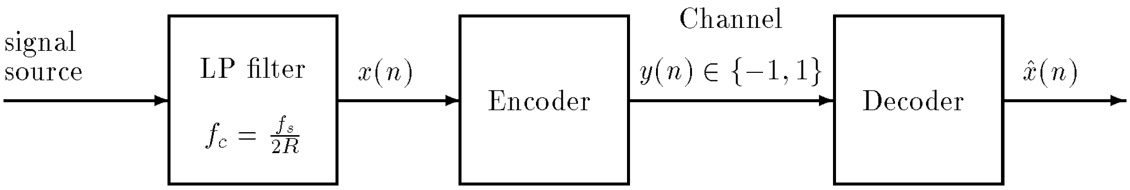

Figure 1.1: Oversampled one-bit signal transmission

by the rate-distortion curve is an upper limit, which is only attained using an optimum choice of encoder and decoder.

In a Pulse Code Modulation (PCM) system, the oversampled signal $x(n)$ is downsampled R times and sampled using a quantizer with 2^{R} levels, i.e., an R-bit quantizer. For a uniform and 'busy' quantizer, the MSE is approx. $\Delta^2/12$ where Δ is the quantization step size [19]. When a system is claimed to have R-bits of resolution, the MSE is similar to that of an R-bit PCM system. In general, resolution is traded for speed, i.e., lower MSE requires a higher oversampling factor R.

The decoding process in a PCM system is generally nonlinear: the incoming bits must be grouped together in order to form R-bit binary words. The significances or weights of the bits depend on the bit position within the word and this makes the decoder nonlinear.

1.2 The Linear Decoding Constraint

The decoder can be designed as a linear system, i.e., the decoder is a filter characterized by a transfer function or an impulse response. The use of linear decoding limits obviously the attainable performance of the transmission system, i.e., the encoder must take the linear decoding into account. The subject of this dissertation is encoders designed for use with an ideal lowpass filter as decoder. The linear decoding constraint makes it impossible to obtain R-bits of performance for R times oversampling.

One-bit encoding for use with linear decoding is very useful for the construction of data converters [9]. If a one-bit encoder is inserted in a general D/A converter, only a simple switch producing a two-level analog signal is needed. The two-level signal is then 'decoded' using an analog reconstruction low-pass filter. This approach simplifies the analog circuitry needed for a converter at the expense of a higher sample rate (R times oversampling) and a more complex digital encoding scheme. In an A/D converter, an analog one-bit encoder can be used as a front-end and the high-rate digital one-bit signal is then decoded using a digital decimation filter. Also in this case, the analog circuitry is simplified at the expense of more complex digital post-processing. Thanks to the rapid progress of digital VLSI technology, the use of oversampling one-bit converters has become widespread.

1.3 Σ-Δ Modulation

The designation Σ-Δ modulation (or Δ-Σ modulation) covers a class of one-bit encoders which is well suited for linear decoding (see [8] and [25] for a general introduction). The first member of this class was the Δ modulator which only needs an integrator for decoding (see Fig. 1.2). A Δ modulator compares the input signal with the integrated encoder output signal and if the input is higher than the integrator output, a $+1$ code is generated. In the opposite case, a -1 code is generated. This primitive type of encoder can only encode the difference (Δ) from sample to sample, hence the name Δ modulation.

The Δ modulator has very poor performance at low frequencies due to the differencing and therefore an integrator could profitably be placed before the Δ modulator. The overall system was named a Σ-Δ modulator due to the Δ modulator being preceded by an integrator (Σ). Using a simple system transformation, the Σ-Δ modulator can be constructed using only one integrator which accumulates the difference between the modulator input and output. This system is shown in Fig. 1.3. The Δ modulator actually contains a

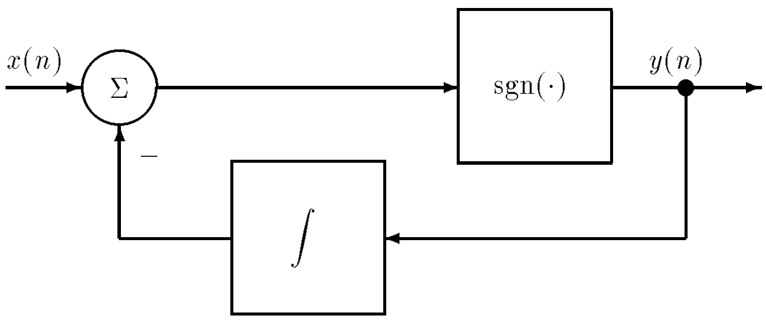

Figure 1.2: Δ modulator. The block marked $\int$ is a discrete-time delaying integrator.

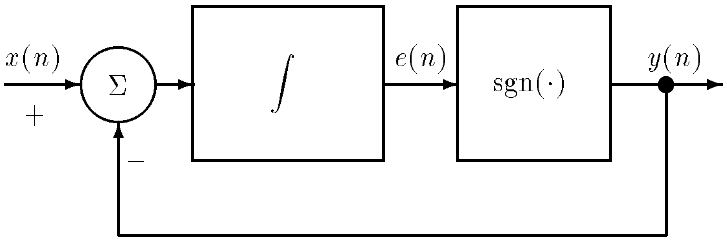

Figure 1.3: First order Σ-Δ modulator. The block marked $\int$ is a discrete-time delaying integrator.

decoder (i.e., an integrator) and the output code decision is based on a comparison of the input and the decoded output, i.e., the encoder is constructed from a decoder using a feedback loop.

The simple discrete-time delaying integrator of Fig. 1.3 with transfer function $1/(z-1)$ can be replaced by a more complex higher order feedback filter with transfer function $H(z)$. The rôle of the filter is unchanged: the filter locally decodes the output code and error feedback is used to generate the output code. The feedback filter output $e(n)$ is the filtered difference between the modulator input and output. The feedback action tries to minimize the magnitude of this error signal. Consequently, if $H(z)$ is a low-pass filter, the coding error will be low for low frequencies due to the feedback. This phenomenon is known as *noise shaping*, i.e., the coding error (quantization noise) is concentrated at higher frequencies where the decoder (a low-pass filter) removes most of the error. For a first order loop filter with a pole at $z = 1$, the MSE is reduced 9 dB for each doubling of the oversampling ratio R [8].

The use of a more complex second order feedback filter was suggested in [8]. This allows a 15 dB reduction in MSE for each doubling of R, i.e., a more selective noise shaping. However, the author of [8] warned that feedback filters containing more than two integrators resulted in unstable modulators.

The stability problem was (and is) a severe obstacle to practical use of higher order Σ-Δ modulators. A major step forward was made by the authors of [10, 34] who proposed a general topology for high-order modulators which was shown to comprise practically useful and stable modulators. There are currently many commercial data converters using high-order modulators [1, 17] based on the pioneering work of [34]. The widespread scepticism about the stability of high-order modulators seems to prevail even despite such commercial devices. However, there are still many issues of the stability problem which need to be clarified.

The general (high-order) Σ-Δ modulator is a useful family of one-bit signal encoders that are constrained by a demand for linear (LP filter) decoding. The demand for stability is another encoder constraint which limits the attainable performance. An obvious question is of course: is it possible to find a better class of encoders which do not suffer from the stability problem?

1.4 Σ-Δ Modulation with Nonlinear Decoding

It has recently been discovered that the use of nonlinear decoding in conjunction with a Σ-Δ modulator as encoder can reduce the MSE compared to linear decoding [25, 39]. The proposed algorithms utilize a more specific knowledge of the non-linear encoding process.

Nonlinear decoding can be useful in A/D data converters where the decoding process is digital. A general nonlinear decoder may also compensate for circuit nonidealities in the analog encoder. However, for D/A converters, the decoding process takes place in the analog domain and this virtually excludes the possibility of nonlinear decoding.

1.5 Overview

The objective of the present dissertation is to clarify the complex issue of modulator stability and present methods for systematic and automated design of practically useful modulators. Everywhere, it is assumed that the used decoding is linear.

The dissertation is divided into two parts. Part I (Ch. 2–5) is devoted to fundamental stability analysis. Ch. 2 introduces the Σ-Δ modulator as a dynamical system using a rather mathematical description. Subsequently, basic properties of dynamical systems are discussed (e.g., *chaos, limit cycles etc.*). The purpose of the mathematical description is to isolate the modulator functionality from the more technological aspects and to provide a solid foundation for later stability analysis. In order to provide a good overview of the many different modulator topologies, the concept of modulator equivalence is introduced.

Ch. 3 focuses on chaotic modulators and various aspects of the onset of instability. The theory is accompanied by numerous examples and a measure of the degree of instability is introduced. Chaotic modulators are interesting for at least two reasons: they produce nonperiodic output and the use of chaos can help to suppress possible spurious tones in the modulator output spectrum. Secondly, the question of stability in conjunction with chaotic modulators is conceptually simpler than for nonchaotic modulators.

Ch. 4 introduces a framework of stability analysis based on symbolic dynamics, i.e., the study of the possible code sequences produced by a modulator.

Ch. 5 focuses on the stability of nonchaotic modulators. It is shown that nonchaotic high-order modulators are very complex and difficult to describe as either stable or unstable.

Part II (Ch. 6–9) presents methods and tools for systematic modulator design and optimization.

Ch. 6 introduces an analysis framework called quasilinear modeling, i.e., the use of linearized models. This chapter is an extension of [49, 51]. The chapter leads to the introduction of an approximate stability criterion.

Ch. 7 presents methods for systematic and automated modulator optimization. Useful constraints are found which ensures the design of stable and reliable modulators. The analysis in this chapter is a synthesis of the results obtained in part I and Ch. 6.

Ch. 8 is devoted to the problem of spurious modulator tones and noise modulation which are highly objectionable adverse effects in audio systems. A comparison of dithering (i.e., the addition of random noise) and the use of chaos for tone suppression is presented in an accompanying paper reprinted in App. A. The similarities between dithering and chaos are pointed out using results from information theory and symbolic dynamics (from Ch. 4).

Ch. 9 introduces a novel modulator topology which comprises a general vector quantizer. This is an attempt to answer the question: is it possible to find better one-bit encoders than Σ-Δ modulators? The use of vector quantization is used to enhance the stability of conventional modulators. This is shown in an accompanying paper reprinted in App. B.

App. C is an independent paper which is based on the methods presented in this dissertation. The paper describes the practical implementation of an entire eighth-order audio D/A converter for 32 times oversampling. Details of both the analog and digital circuitry are presented along with theory concerning possible error sources in D/A conversion (e.g., clock jitter and inter symbol interference).

Part I

Fundamental Analysis

Chapter 2

The Σ-Δ Modulator as a Dynamical System

2.1 Introduction

Σ-Δ modulators in analog-to-digital or digital-to-analog converters can be implemented in many ways; there are especially many different approaches related to different technologies: some designs are based on continuous time circuits and others are based on discrete-time switched capacitor or even switched current techniques. In addition, many different topologies are used.

This diversity of real implementations makes it at first sight very difficult to describe and analyze Σ-Δ modulators as one class of systems. In order to be able to understand and analyze such complex systems it is absolutely necessary to use a description which is technology independent. Therefore, a more mathematical approach, i.e., the concept of *nonlinear dynamical systems* will be introduced in the next sections. This will probably be regarded as just another way to introduce confusion by many readers not familiar with such mathematical description. The real purpose is, however, to give the reader a better overview and ability to see through different implementations. For instance, many seemingly different circuits can in fact be equivalent, i.e., they do the same signal processing but are implemented differently.

The mathematical description is especially useful for the design of Σ-Δ modulators: at first the modulator is optimized for functionality in the mathematical domain and, subsequently, the design is transferred to real circuit elements.

2.2 Introducing Dynamical Systems

In this section, a brief introduction to time-discrete dynamical systems will be given.

A given discrete-time dynamical system is characterized by a state-space S and two mappings $\mathcal{F} : S \times I \to S$ and $\mathcal{O} : S \to O$. The state-space is the set of possible states of the system and the $\mathcal{F}$ mapping describes the next state as a function of the current state and an independent system input taken from the set I. The output mapping $\mathcal{O}$ generates the system output as a function of the current system state and input:

$$\begin{aligned} \boldsymbol{x}_{n+1} &= \mathcal{F}(\boldsymbol{x}_n, \boldsymbol{i}_n) \quad , \mathcal{F} : S \times I \to S \\ \boldsymbol{o}_n &= \mathcal{O}(\boldsymbol{x}_n, \boldsymbol{i}_n) \quad , \mathcal{O} : S \times I \to O \end{aligned} \tag{2.1}$$

where $\boldsymbol{x}_n \in S$, $\boldsymbol{i}_n \in I$ and $\boldsymbol{o}_n \in O$ are the system state, input and output at time-step n, respectively.

An Nth order system can be described by N independent state-coordinates which form an N-dimensional state-space. The chosen state-coordinates will generally describe physical properties of the system, e.g., voltages in circuit nodes, physical displacements, etc. The choice of state-coordinates for a given system is ambiguous, i.e., a multitude of different state-space descriptions of the same system can be given corresponding to different choices of independent state-variables. All of these state-space descriptions result in the same output signal sequence for the same input signal sequence. Generally, two state-space description of the same system have state-coordinates which are related through a one-to-one (bijective) transform $\mathcal{T}$. This fact motivates following definition:

Definition 2.1 *Two dynamical systems described by the maps $\mathcal{F}_1 : S_1 \times I \to S_1$, $\mathcal{O}_1 : S_1 \times I \to O$, $\mathcal{F}_2 : S_2 \times I \to S_2$ and $\mathcal{O}_2 : S_2 \times I \to O$, are defined as being* equivalent *if and only if a one-to-one map $\mathcal{T} : S_2 \to S_1$ exists satisfying:*

$$\begin{aligned} \mathcal{F}_2(\boldsymbol{y}_n, \boldsymbol{i}_n) &= \mathcal{T}^{-1}(\mathcal{F}_1(\mathcal{T}(\boldsymbol{y}_n), \boldsymbol{i}_n)) \, , \, \boldsymbol{y}_n \in S_2 \\ \mathcal{O}_2(\boldsymbol{y}_n, \boldsymbol{i}_n) &= \mathcal{O}_1(\mathcal{T}(\boldsymbol{y}_n), \boldsymbol{i}_n) \end{aligned} \tag{2.2}$$

The dynamical systems discussed so far, as described by Eq. (2.1), have been operating with an independent input signal sequence. A certain subset of the dynamical systems are the so-called autonomous systems which operate without input.

The sequence of states corresponding to time step n for an autonomous system is thus given by applying a mapping $\mathcal{F} : S \to S$ iteratively on an initial state $\boldsymbol{x}_0 \in S$:

$$\boldsymbol{x}_n = \mathcal{F}^n(\boldsymbol{x}_0) \, , \, n \in \mathbb{N} \tag{2.3}$$

Consequently, the study of the dynamics of autonomous systems is equivalent to the study of the iterations of a mapping. In fact, Eq. (2.3) defines a mapping between the initial state and the output state sequence which is called the *orbit* corresponding to the initial state $\boldsymbol{x}_0$, i.e., the sequence $\{\boldsymbol{x}_n\}_{n=0}^{\infty}$.

If the input signal of a given nonautonomous system can be generated from an autonomous system, the nonautonomous system and the input generating system can be merged into a single autonomous system. Especially, systems with constant input signal can generally be described as autonomous when the constant input is 'built' into the $\mathcal{F}$ mapping. This procedure will be used extensively in the following.

2.3 Basic Properties of Dynamical Systems

The discussion on dynamical systems will be focused on autonomous time-discrete systems cf. Eq. (2.3). Recall, that the initial condition $\boldsymbol{x}_0$ defines the orbit of the system. The *steady state* of a system refers to the asymptotic behavior as $n \to \infty$. The difference between the orbit and the steady state is called the *transient*. The following definitions are from [46]:

2.3.1 Limit Sets

Definition 2.2 *A point $\boldsymbol{y}$ of $\boldsymbol{x}_0$ for the map $\mathcal{F}$ is called a* limit point *of $\boldsymbol{x}_0$ if, for every neighborhood O of $\boldsymbol{y}$, the orbit $\mathcal{F}^n(\boldsymbol{x}_0)$ repeatedly enters O as $n \to \infty$.*

The set $L(\boldsymbol{x}_0)$ of all limit points of $\boldsymbol{x}_0$ is called the limit set *of $\boldsymbol{x}_0$.*

The limit set L of an initial condition $\boldsymbol{x}_0$ is the set in state-space the orbit visits frequently in steady state. In other words: a limit set characterizes a steady-state solution. A fundamental property of linear systems is that there is either one limit set or infinitely many limit sets. Nonlinear system may have a finite number of coexisting limit sets.

Definition 2.3 *A limit set L is* attracting *or* asymptotically stable *if there exists an open neighborhood O of L such that $L(\boldsymbol{x}) = L$ for all $\boldsymbol{x} \in O$. The union of all such neighborhoods O is called the* basin of attraction B_L *of an attracting limit set L.*

The basin of attraction is the set of points which are asymptotically attracted to the limit set. Stable linear systems have only one limit set. Furthermore, the limit set is attracting and the basin of attraction is the entire state-space, i.e., the limit set of a stable linear system is *globally attracting.*

Definition 2.4 *A* fixed point *or a* equilibrium point *$\boldsymbol{x}^*$ of a map $\mathcal{F}$ is a point for which $\mathcal{F}(\boldsymbol{x}^*) = \boldsymbol{x}^*$. The limit set of a fixed point is the fixed point itself.*

Stable linear systems with constant input have precisely one fixed point and this fixed point is the only limit set.

Definition 2.5 *A* periodic point *$\boldsymbol{x}^p$ of a map $\mathcal{F}$ is a point for which a number $k \in \mathbb{N}$ exists satisfying $\mathcal{F}^k(\boldsymbol{x}^p) = \boldsymbol{x}^p$. The least number K for which $\mathcal{F}^K(\boldsymbol{x}^p) = \boldsymbol{x}^p$, is called the* prime period *of the periodic point. A periodic point with prime period K is called a period-K point. The closed orbit $\{\boldsymbol{x}^p, \mathcal{F}(\boldsymbol{x}^p), \ldots \mathcal{F}^K(\boldsymbol{x}^p)\}$ is called a* limit cycle *or a* periodic orbit *which is the limit set of the period-K point.*

2.3.2 The Stability of Fixed and Periodic points

The stability of fixed points and periodic points can be studied by linearization. Let $\boldsymbol{x}^*$ be a fixed point of a map $\mathcal{F}$. The orbit $\boldsymbol{x}_n$ corresponding to the initial condition $\boldsymbol{x}^* + \delta\boldsymbol{x}_0$ can then be approximated to first order by:

$$\boldsymbol{x}_n = \mathcal{F}^n(\boldsymbol{x}^* + \delta\boldsymbol{x}_0) \approx \boldsymbol{x}^* + (\mathrm{D}\mathcal{F}|_{\boldsymbol{x}^*})^n \delta\boldsymbol{x}_0 \tag{2.4}$$

where $\mathrm{D}\mathcal{F}|_{\boldsymbol{x}^*}$ is the functional (Jacobian) matrix of $\mathcal{F}$, i.e. a matrix with the $N \times N$ partial derivatives evaluated at $\boldsymbol{x} = \boldsymbol{x}^*$.

The stability of the orbit, cf. Eq. (2.4), can in some cases be determined by the eigenvalues $\{\lambda_i\}$ of the linearized system, i.e. the eigenvalues of $\mathrm{D}\mathcal{F}|_{\boldsymbol{x}^*}$. If $|\lambda_i| < 1$ for all i then all sufficiently small perturbations will tend toward zero as $n \to \infty$, and the fixed point is attracting or asymptotically stable. Conversely, if any of the eigenvalues has modulus greater than unity, then perturbations in certain directions will grow with time, and the fixed point is consequently unstable.

Since a period-K point $\boldsymbol{x}^p$ of a map $\mathcal{F}$ is a fixed point of the map $\mathcal{F}^K$, the stability of limit cycles can be determined from the eigenvalues of $\mathrm{D}\mathcal{F}^{\mathrm{K}}(\boldsymbol{x})$. Using the chain rule:

$$\mathrm{D}\mathcal{F}^{\mathrm{K}}|_{\boldsymbol{x}^{\mathrm{p}}} = \mathrm{D}\mathcal{F}|_{\boldsymbol{x}_{\mathrm{K}-1}} \cdot \mathrm{D}\mathcal{F}|_{\boldsymbol{x}_{\mathrm{K}-2}} \cdots \mathrm{D}\mathcal{F}|_{\boldsymbol{x}_0} \tag{2.5}$$

where $\boldsymbol{x}_i = \mathcal{F}^i(\boldsymbol{x}^p)$ is the corresponding orbit or limit cycle.

2.3.3 Chaos

Some nonlinear dynamical systems have asymptotic orbits that are completely nonperiodic. This can be the case when the orbit can be dissolved into a countable sum of periodic functions each of whose periods are an integer combination of frequencies taken from a finite base set [46]. Such asymptotic behavior is called *quasiperiodic* and the orbits are nonperiodic but predictable on any time scale. For instance, the sum of two sine waves with incommensurable frequencies is nonperiodic but easily predictable. Even a single discrete-time sinusoidal signal with irrational frequency is nonperiodic.

In some cases a nonlinear dynamical system can exhibit another nonperiodic steady state behavior called *chaos*. Chaos can loosely be defined as a nonperiodic motion that is not quasiperiodic, i.e., a chaotic orbit cannot be described by a finite number base frequencies and the orbit cannot be predicted on long time scales. There is no commonly accepted definition for chaos but most definitions have the same ingredients stated in different ways. Most definitions require at least the first two of the following three properties to be fulfilled: A system map $\mathcal{F}$ is chaotic on a domain L if

1. There is a sensitivity to initial conditions, i.e., two nearby orbits diverge and will eventually become uncorrelated. This makes long term prediction impossible.

2. The system map is topologically transitive on L, i.e., points within any given neighborhood of L can eventually hit any point in L. This basically ensures that the entire domain L is visited repeatedly, i.e., L is actually a limit set, cf. Definition 2.2.

3. The periodic points are dense in L, i.e., every neighborhood of a point in L contains at least one periodic point.

Such mathematical definitions do not guarantee the existence of a nonperiodic solution. However, for most nice systems, fulfilling the above requirements, there will be a nonperiodic *dense orbit* that comes arbitrarily close to any point in the limit set.

A chaotic limit set is from a practical point of view just the union of infinitely many unstable limit cycles. A given initial point can always be perturbed slightly in order to get a periodic orbit of some period length. A chaotic limit set cannot contain any stable limit cycles since each stable limit cycle forms a stable limit set with a corresponding basin of attraction where there is no sensitivity to initial conditions.

A chaotic orbit is always close to many limit cycles but the orbit will be nonperiodic since every limit cycle is repelling. The unstable limit cycles will therefore form the skeleton of a chaotic limit set: the short cycles shows the basic structure and the longer cycles add more details [13]. Chaotic limit sets are often very complex geometric objects with a fractal dimension. A stable and fractal limit set is often called a *strange attractor*.Conversely, an asymptotically unstable chaotic and fractal limit set is a *strange repeller*.

2.4 The Σ-Δ Modulator

A Σ-Δ modulator is a linear filter with a binary feedback signal formed as the negated sign of the filter output (see Fig. 2.1). A linear and causal Nth order filter is a dynamical system as described by Eq. (2.1) for which the state-space is the Euclidean space, $S = \mathbb{R}^N$, and both of the mappings $\mathcal{F}$ and $\mathcal{O}$ are linear. The linear filter $H(z)$ in Fig. 2.1 can thus

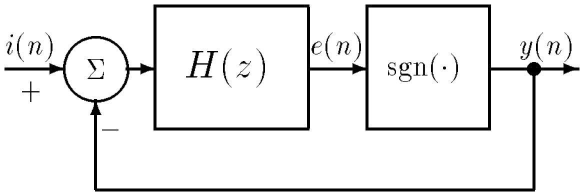

Figure 2.1: Σ-Δ modulator.

be described in state-space as follows [18]:

$$\begin{aligned} \boldsymbol{x}_{n+1} &= \boldsymbol{A}\boldsymbol{x}_n + \boldsymbol{b}i(n) \\ e(n) &= \boldsymbol{c}^\top \boldsymbol{x}_n + di(n) \end{aligned} \tag{2.6}$$

Where $i(n)$ and $e(n)$ are the (scalar) filter input and output signals, respectively. The transition matrix $\boldsymbol{A}$ is an (N, N) matrix and $\boldsymbol{b}$, $\boldsymbol{c}$ and the state vector $\boldsymbol{x}_n$ are column vectors of length N. The parameter d determines obviously the impulse response value at time zero, i.e., $h(0) = d$. The transfer function $H(z)$ of the filter can be found from Eq. (2.6) using the z-transform and linear algebra:

$$\begin{aligned} z\boldsymbol{X}(z) &= \boldsymbol{A}\boldsymbol{X}(z) + \boldsymbol{b}\boldsymbol{I}(z) \ \Rightarrow \\ \boldsymbol{X}(z) &= -(\boldsymbol{A} - \boldsymbol{E}z)^{-1}\boldsymbol{b}I(z) \\ E(z) &= \boldsymbol{c}^\top \boldsymbol{X}(z) + dI(z) \\ &= H(z)I(z) = (d - \boldsymbol{c}^\top(\boldsymbol{A} - \boldsymbol{E}z)^{-1}\boldsymbol{b})I(z) \end{aligned} \tag{2.7}$$

Where $\boldsymbol{X}(z)$, $E(z)$ and $I(z)$ are the z-transforms of the state vector sequence $\boldsymbol{x}_n$ and the filter output and input, respectively. The matrix $\boldsymbol{E}$ is the (N, N) unit matrix.

Eq. (2.7) shows that the poles of $H(z)$ are the z-values for which Eq. (2.7) becomes singular, i.e., the poles of $H(z)$ are equal to the roots of the characteristic polynomial of $\boldsymbol{A}$. In other words, the eigenvalues of $\boldsymbol{A}$ are poles of $H(z)$. The zeros of $H(z)$ are generally determined by $\boldsymbol{b}$, $\boldsymbol{c}$ and d.

For a given state-space description of a filter, the transfer function will be uniquely determined by Eq. (2.7); however, a multitude of state-space descriptions result in a given transfer function. A well known result from linear system theory is that two filters with the same transfer function generate identical output for identical input when proper initial conditions are used, i.e., filters with identical transfer function $H(z)$ are equivalent, cf. Definition 2.1.

Using Eq. (2.6), an Nth order Σ-Δ modulator corresponding to Fig. 2.1 can be characterized in state-space matrix-vector notation:

$$\begin{aligned} \boldsymbol{x}_{n+1} &= \boldsymbol{A}\boldsymbol{x}_n + \boldsymbol{b}(i(n) - \mathrm{sgn}(\boldsymbol{c}^\top \boldsymbol{x}_n)),\ \boldsymbol{x}_n \in \mathbb{R}^N \\ y(n) &= \mathrm{sgn}(\boldsymbol{c}^\top \boldsymbol{x}_n) \end{aligned} \tag{2.8}$$

where $y(n)$ is the modulator output sequence and $\mathrm{sgn}(\cdot)$ denotes the signum function, i.e., $\mathrm{sgn}(x) \triangleq 1$ for positive x and $\mathrm{sgn}(x) \triangleq -1$, otherwise.

Using the system description of Eq. (2.1), this general Nth order Σ-Δ modulator can be characterized by:

$$\begin{aligned} \boldsymbol{x}_{n+1} &= \mathcal{F}(\boldsymbol{x}_n, i(n)) = \boldsymbol{A}\boldsymbol{x}_n + \boldsymbol{b}(i(n) - \mathcal{O}(\boldsymbol{x}_n)) \\ y(n) &= \mathcal{O}(\boldsymbol{x}_n) = \operatorname{sgn}(\boldsymbol{c}^\top \boldsymbol{x}_n) \end{aligned} \tag{2.9}$$

The feedback loop of Fig. 2.1 including the signum function cannot be realized if the filter is delay free, i.e., the filter impulse response must have the property $h(0) = 0$, where $h(n)$ is the impulse reponse of $H(z)$. This is the reason why the parameter d from Eq. (2.6) is omitted in Eq. (2.8).

For most Σ-Δ modulator topologies, the feedback filter transfer function $H(z)$ is not immediately observable. In these cases, the modulator has to be described in state-space at first before $H(z)$ can be derived using Eq. (2.7).

Example 2.1 Consider the second order modulator of Fig. 2.2 with three parameters, b_1, b_2 and a. The feedback filter is composed of a cascade of discrete-time integrators with distributed input. This approach is extensively used for construction of high-order modulators [1, 55, 17] and the resulting coefficient sensitivity is low compared to other structures [49]. The two variables $x_1(n)$ and $x_2(n)$ are chosen as state-coordinates, i.e., the state-vector is $\boldsymbol{x}_n = \begin{bmatrix} x_1(n) & x_2(n) \end{bmatrix}^\top$. This choice results in the following state-space description:

$$\begin{aligned} \boldsymbol{x}_{n+1} &= \boldsymbol{A}\boldsymbol{x}_n + \boldsymbol{b}\left(i(n) - \operatorname{sgn}\left(\boldsymbol{c}^\top \boldsymbol{x}_n\right)\right) \\ \boldsymbol{A} &= \begin{bmatrix} 1 & 1 \\ -a & 1 \end{bmatrix} \\ \boldsymbol{b} &= \begin{bmatrix} b_1 & b_2 \end{bmatrix}^\top \\ \boldsymbol{c} &= \begin{bmatrix} 1 & 0 \end{bmatrix}^\top \end{aligned} \tag{2.10}$$

The feedback transfer function $H(z)$ can now be derived using Eq. (2.7):

$$\begin{aligned} H(z) &= -\boldsymbol{c}^\top (\boldsymbol{A} - \boldsymbol{E}z)^{-1} \boldsymbol{b} \\ &= \begin{bmatrix} 1 & 0 \end{bmatrix} \frac{-1}{z^2 - 2z + 1 + a} \begin{bmatrix} 1-z & -1 \\ a & 1-z \end{bmatrix} \begin{bmatrix} b_1 \\ b_2 \end{bmatrix} \\ &= \frac{b_1 z^{-1} + (b_2 - b_1) z^{-2}}{1 - 2z^{-1} + (1+a) z^{-2}} \end{aligned} \tag{2.11}$$

Notice that b_1 and b_2 determine the zero of $H(z)$ and that $H(z)$ has the required unit sample delay. The poles of $H(z)$ are determined alone by the internal feedback factor a □

2.5 Σ-Δ Modulator Equivalences

As stated in Sec. 2.4, two linear dynamical systems are equivalent if they have identical transfer functions. Consequently, two Σ-Δ modulators are equivalent if the corresponding feedback filters have identical transfer functions. Furthermore, Σ-Δ modulators are

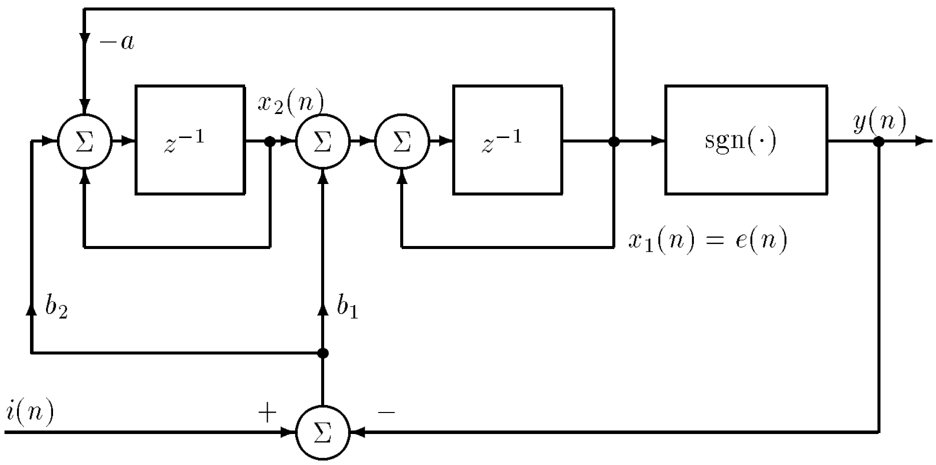

Figure 2.2: Second order Σ-Δ modulator example.

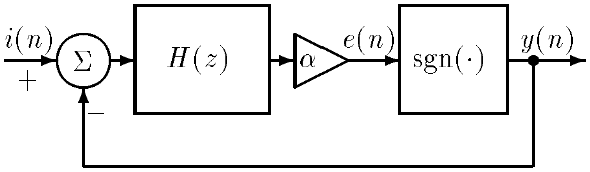

Figure 2.3: Σ-Δ modulator with feedback filter scaling.

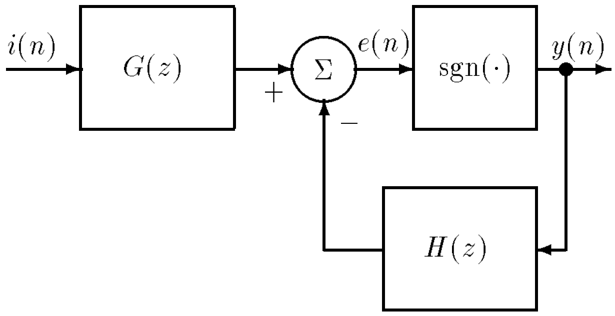

Figure 2.4: Generic Σ-Δ modulator.

invariant to scaling of the feedback filter $H(z)$. This fact can be realized from Fig. 2.3 where the filter output is scaled by the factor α before the signum function. This system produces obviously the same output for any positive value of α due the fact that the signum function is invariant to argument scaling. This justifies the following theorem:

Theorem 2.1 *Two Σ-Δ modulators cf. Fig. 2.1 are equivalent if and only if the corresponding feedback filters $H_1(z)$ and $H_2(z)$ have the property:*

$$H_2(z) = \alpha H_1(z) \ , \ \alpha > 0 \tag{2.12}$$

The theorem states that the poles and zeros of $H(z)$ defines two equivalence classes of modulators giving the same output for the same input, i.e., one class for negative and one class for positive scalings of $H(z)$.

Example 2.2 Consider the modulator in Fig. 2.2 discussed in Example 2.1. Since the modulator is invariant to scalings of $H(z)$, it is observed from Eq. (2.11) that the parameter b_1 can be fixed to unity without loss of generality, i.e., the real valued zero of $H(z)$ can be determined alone by the remaining parameter b_2. Scaling of both b_1 and b_2 will only affect the internal signal levels within the integrators. The actual scaling can be decided when the circuit is to be implemented □

So far, the modulators considered have been restricted to a certain class as defined by Fig. 2.1 which does not comprise every known modulator topology. Fig. 2.4 shows a more general generic Σ-Δ modulator which is characterized by two transfer functions, i.e., the feedback filter $H(z)$ between the quantizer output and input and the input transfer function $G(z)$ between the input and the quantizer input. The generic modulator of Fig. 2.4 can be rearranged into an equivalent system consisting of a usual modulator cf. Fig. 2.1 preceded by a linear prefilter as shown in Fig. 2.5. Consequently, generic

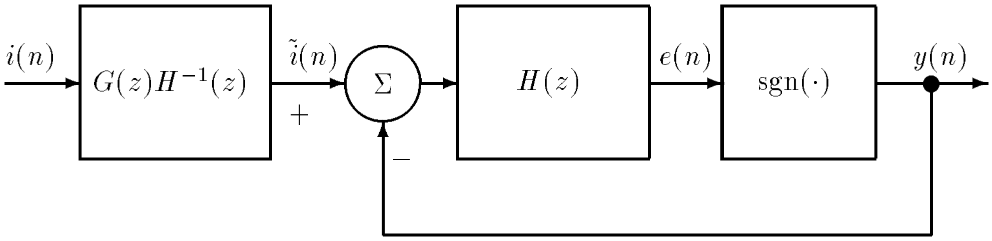

Figure 2.5: Generic Σ-Δ modulator implemented as a usual modulator with a prefilter.

modulators cf. Fig. 2.4 with the same feedback filter $H(z)$ are equivalent when the input signal is preprocessed by a proper linear filter. Since linear filtering is a very well known operation, the study of the nonlinear dynamics of Σ-Δ modulators can be restricted to the sub-class cf. Fig. 2.1. Notice that generic modulators are generally not invariant to scalings of $H(z)$ since the the prefilter $G(z)H^{-1}(z)$ scales inversely with $H(z)$.

Example 2.3 Consider the second order modulator in Fig. 2.6. This modulator topology is a modification of the modulator shown in Fig. 2.2 and is commonly know as the *multiple feedback* modulator [55]. This example will demonstrate that the multiple feedback modulator is comprised by the generic model, cf. Fig. 2.4.

Obviously, the modulators of Fig. 2.2 and Fig. 2.6 share the same feedback filter $H(z)$, cf. Eq. (2.11):

$$H(z) = \frac{b_1 z^{-1} + (b_2 - b_1) z^{-2}}{1 - 2z^{-1} + (1+a)z^{-2}} \tag{2.13}$$

The input transfer function, $G(z)$, from the input node to the quantizer input node is found:

$$\begin{aligned} G(z) &= -\boldsymbol{c}^\top (\boldsymbol{A} - \boldsymbol{E}z)^{-1} \begin{bmatrix} 0 & 1 \end{bmatrix}^\top \\ &= \frac{z^{-2}}{1 - 2z^{-1} + (1+a)z^{-2}} \end{aligned} \tag{2.14}$$

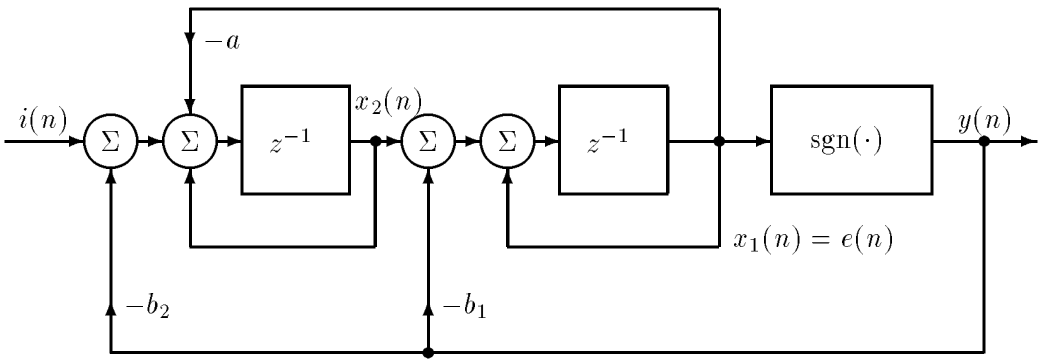

Figure 2.6: Second-order multiple feedback Σ-Δ modulator.

Consequently, the multiple feedback modulator, cf. Fig. 2.6 is equivalent to the modulator in Fig. 2.2 preceded by the prefilter:

$$G(z)H^{-1}(z) = \frac{z^{-2}}{b_1 z^{-1} + (b_2 - b_1)z^{-2}} = \frac{1/b_1 z^{-1}}{1 + (b_2/b_1 - 1)z^{-1}} \tag{2.15}$$

The prefilter is a first order recursive filter with a one sample delay. Notice also that scaling of both b_1 and b_2 just scales the gain of the prefilter accordingly.

The multiple feedback modulator is often used in a transposed form called the *feedforward* (FF) modulator [55, 17]. The FF modulator is, like the topology in Fig. 2.2, equivalent to a usual Σ-Δ modulator, i.e., $G(z) = H(z)$ for these topologies □

The subject of equivalences among different modulator topologies has also been discussed in [63, 66, 68].

2.6 The Noninvertible Region

Real physical dynamical systems (e.g., systems ruled by Newton's laws of motion) are reversible, i.e., the axis of time can be reversed. Even when such continuos-time systems a modeled in discrete-time, the system maps are generally invertible and it is possible to go back and forth in time. This section will show that the signum function or one-bit quantizer of a Σ-Δ modulator causes the system map to be noninvertible in a certain region in the state-space.

The nonlinear map $\mathcal{F}$ of a Σ-Δ modulator with constant input i can be characterized by two linear maps defined on two distinct domains:

$$\mathcal{F}(\boldsymbol{x}_n) = \begin{cases} \mathcal{F}_+(\boldsymbol{x}_n) & , \boldsymbol{x}_n \in S_+ \\ \mathcal{F}_-(\boldsymbol{x}_n) & , \boldsymbol{x}_n \in S_- \end{cases}$$

$$
\begin{aligned}
S_+ &= \{\boldsymbol{x} \in \mathrm{IR}^N | \mathcal{O}(\boldsymbol{x}) = 1\} \\
&= \{\boldsymbol{x} \in \mathrm{IR}^N | \boldsymbol{c}^\top \boldsymbol{x} > 0\} \\
S_- &= \{\boldsymbol{x} \in \mathrm{IR}^N | \mathcal{O}(\boldsymbol{x}) = -1\} \\
&= \{\boldsymbol{x} \in \mathrm{IR}^N | \boldsymbol{c}^\top \boldsymbol{x} \leq 0\} \\
\mathcal{F}_+(\boldsymbol{x}_n) &= \boldsymbol{A}\boldsymbol{x}_n + \boldsymbol{b}(i-1) \\
\mathcal{F}_-(\boldsymbol{x}_n) &= \boldsymbol{A}\boldsymbol{x}_n + \boldsymbol{b}(i+1)
\end{aligned} \tag{2.16}
$$

The piecewise linearity enables the existence of a region U in which the system map is noninvertible, i.e., U is the set of elements $\boldsymbol{y}$ which gives two solutions to the equation $\mathcal{F}(\boldsymbol{x}) = \boldsymbol{y}$. Since both of the linear maps $\mathcal{F}_+$ and $\mathcal{F}_-$ are generally invertible, the set U can be derived:

$$
\begin{aligned}
U &= \mathcal{F}_+(S_+) \bigcap \mathcal{F}_-(S_-) \\
&= \{\boldsymbol{y} \in \mathrm{IR}^N | \mathcal{F}_+^{-1}(\boldsymbol{y}) \in S_+ \wedge \mathcal{F}_-^{-1}(\boldsymbol{y}) \in S_-\} \\
&= \{\boldsymbol{y} \in \mathrm{IR}^N | \boldsymbol{c}^\top \boldsymbol{A}^{-1}\boldsymbol{b}(i-1) < \boldsymbol{c}^\top \boldsymbol{A}^{-1}\boldsymbol{y} < \boldsymbol{c}^\top \boldsymbol{A}^{-1}\boldsymbol{b}(i+1)\}
\end{aligned} \tag{2.17}
$$

Both the sets $V_+ = \mathcal{F}_+^{-1}(U)$ and $V_- = \mathcal{F}_-^{-1}(U)$ are mapped on U by $\mathcal{F}$, i.e., the set $V = V_+ \bigcup V_-$ is the preimage of the noninvertible region U. The set V has a remarkably simple structure:

$$
\begin{aligned}
V_+ &= \{\boldsymbol{x} \in \mathrm{IR}^N | \boldsymbol{c}^\top \boldsymbol{A}^{-1}\boldsymbol{b} < \boldsymbol{c}^\top \boldsymbol{A}^{-1}\left(\boldsymbol{A}\boldsymbol{x} + \boldsymbol{b}(i-1)\right) < \boldsymbol{c}^\top \boldsymbol{A}^{-1}\boldsymbol{b}(i-1)\} \\
&= \{\boldsymbol{x} \in \mathrm{IR}^N | 0 < \boldsymbol{c}^\top \boldsymbol{x} < 2\boldsymbol{c}^\top \boldsymbol{A}^{-1}\boldsymbol{b}\} \\
V_- &= \{\boldsymbol{x} \in \mathrm{IR}^N | -2\boldsymbol{c}^\top \boldsymbol{A}^{-1}\boldsymbol{b} < \boldsymbol{c}^\top \boldsymbol{x} < 0\} \\
V &= \{\boldsymbol{x} \in \mathrm{IR}^N | \, |\boldsymbol{c}^\top \boldsymbol{x}| < 2\boldsymbol{c}^\top \boldsymbol{A}^{-1}\boldsymbol{b}\}
\end{aligned} \tag{2.18}
$$

Recall from Sec. 2.4 that the quantizer input e is equal to $\boldsymbol{c}^\top \boldsymbol{x}$ and that the transfer function of the feedback filter is given by $H(z) = -\boldsymbol{c}^\top(\boldsymbol{A} - \boldsymbol{E}z)^{-1}\boldsymbol{b}$. Consequently, the elements in V satisfy the very simple relation:

$$
|e| < -2H(z=0) \tag{2.19}
$$

Notice that this relation is very general, i.e., V is independent of the modulator input signal and V is defined only by the observable quantizer input e and by the feedback filter $H(z)$. It can be concluded that if a modulator operates exclusively in the noninvertible region U, it must operate exclusively in V as well, i.e., the quantizer input magnitude will be bounded by $-2H(z=0)$. Notice furthermore that U is nonempty for $H(z=0) < 0$. It will be demonstrated later that the noninvertible region plays an important rôle for the stability of a modulator.

2.7 Local Stability Analysis and Limit Cycle Identification

This section focuses on the structure and stability of the limit cycles of Σ-Δ modulators. The fact that a Σ-Δ modulator is a linear filter with nonlinear and binary feedback simplifies both the identification and stability analysis of possible limit cycles.

According to Eq. (2.16), the functional (Jacobian) matrix of a modulator map is simply given as:

$$
\mathrm{D}\mathcal{F}(\boldsymbol{x}) = \boldsymbol{A} \, , \, \boldsymbol{c}^\top \boldsymbol{x} \neq 0 \tag{2.20}
$$

This means that the eigenvalues of the transition matrix $\boldsymbol{A}$ determines the stability of fixed and periodic points. Recall from Sec. 2.4 that the eigenvalues of $\boldsymbol{A}$ are equal to the poles of the modulator feedback filter $H(z)$. Consequently, modulators with one or more poles outside the unit circle have unstable fixed points and limit cycles.

The limit cycles of a Σ-Δ modulator with known (periodic or constant) input can be identified by opening the modulator loop. This is again a consequence of the feedback path being a linear filter: Consider the modulator of Fig. 2.1 where the loop is opened and the quantizer is replaced by a signal generator which produces a periodic binary signal $y(n)$ with the two discrete amplitude values 1 and -1. The output $e(n)$ of the linear feedback filter $H(z)$ (which formerly was the quantizer input) will then have a periodic steady-state solution and if $\mathrm{sgn}(e(n)) = y(n)$ for all n, a limit cycle exists with $y(n)$ as periodic output code. This means that there is a close relationship between the periodic output code sequence and the limit cycle in state-space.

The periodic steady-state quantizer input signal $e(n)$ can be found as the solution to a set of linear equations for any period k code sequence $y(n)$ and there will thus exist a linear mapping between $y(n)$ and $e(n)$ which depends on $H(z)$ and on the modulator input.

Let $H(z)$ be given as a rational transfer function $C(z)/D(z)$ where $C(z) = c_1 z^{-1} + c_2 z^{-2} \cdots c_N z^{-N}$ and $D(z) = 1 + d_1 z^{-1} + d_2 z^{-2} \cdots d_N z^{-N}$. For a given input signal $i(n)$ and output signal $y(n)$, the loop filter input is given by $v(n) = i(n) - y(n)$. In the z-domain, the loop filter output $e(n)$ is given by:

$$E(z) = \frac{C(z)}{D(z)} V(z) \tag{2.21}$$

or equivalently:

$$D(z)E(z) = C(z)V(z) \tag{2.22}$$

Let $v(n)$ be periodic with period k. The steady-state $e(n)$ is then also periodic with period k and $e(n)$ can be found from the following linear equation:

$$\begin{bmatrix} 1 & 0 & \cdots & d_N & \cdots & d_2 & d_1 \\ d_1 & 1 & 0 & \cdots & d_N & \cdots & d_2 \\ \vdots & \vdots & \vdots & \vdots & \vdots & \vdots & \vdots \\ 0 & \cdots & d_N & \cdots & d_3 & d_2 & 1 \end{bmatrix} \begin{bmatrix} e(0) \\ e(1) \\ \vdots \\ e(k-1) \end{bmatrix} =$$

$$\begin{bmatrix} 0 & \cdots & c_N & \cdots & c_2 & c_1 \\ c_1 & 0 & \cdots & c_N & \cdots & c_2 \\ \vdots & \vdots & \vdots & \vdots & \vdots & \vdots \\ 0 & c_N & \cdots & c_2 & c_1 & 0 \end{bmatrix} \begin{bmatrix} v(0) \\ v(1) \\ \vdots \\ v(k-1) \end{bmatrix} \tag{2.23}$$

Or using the symbolic notation:

$$\boldsymbol{D}_k \boldsymbol{e} = \boldsymbol{C}_k \boldsymbol{v} \tag{2.24}$$

The solution is then given by:

$$\boldsymbol{e} = \boldsymbol{D}_k^{-1} \boldsymbol{C}_k \boldsymbol{v} \tag{2.25}$$

The existence of the periodic sequence $y(n)$ as a limit cycle can then be tested using the condition $y(n) = \mathrm{sgn}(e(n))$ for all n.

For certain $H(z)$ pole configurations the set of equations (Eq. (2.23)) may become singular, e.g., if $H(z)$ has a pole a $z = 1$ the filter has infinite dc-gain and the mean value of the filter input must be zero. In this case the mean value of the steady-state filter output is undetermined and may be considered as a free parameter, i.e., there are infinitely many steady-state solutions for $e(n)$. The code sequence will then exist as a limit cycle for the mean value of the filter output belonging to a whole interval where the condition $\mathrm{sgn}(e(n)) = y(n)$ is satisfied for all n. Generally, the steady-state filter output solution is nonunique when one or more $H(z)$ poles are on the unit circle at the locations $\exp(j\pi l/k)$ which correspond to the possible discrete frequencies of the spectra of signals with period k [25]. In these cases, there will either be none or infinitely many solutions.

In order to simplify notation, code sequences will be written as binary numbers, i.e., sequences of the symbols '1' and '0' corresponding to quantizer output amplitudes 1 and -1, respectively. A periodic repetition of a code sequence is indicated by overlining, e.g., the notation $\overline{1100}$ means the (infinite) code sequence 110011001100.... This means that the set of 2^k k-digit binary numbers is equivalent to the set of output sequences with period k and that each possible periodic point can be identified with a binary number. However, normally only a fraction of the 2^k period k sequences will exist as limit cycles.

Code sequence segments can also be described by counting the maximum number of consecutive '1' and '0' symbols. The notation (2,2) means a code segment of two '1' symbols followed by two '0' symbols and the notation $(\overline{2,2})$ is an alternative notation for the periodic sequence $\overline{1100}$.

Example 2.4 Some periodic code sequences with period 4 will be tested for existence as limit cycles for the second-order modulator of Fig. 2.2. The feedback filter $H(z)$ for this modulator is given as (cf. Eq. (2.11)):

$$H(z) = \frac{b_1 z^{-1} + (b_2 - b_1) z^{-2}}{1 - 2z^{-1} + (1+a) z^{-2}} \tag{2.26}$$

The matrix $\boldsymbol{D}_4$ is:

$$\boldsymbol{D}_4 = \begin{bmatrix} 1 & 0 & 1+a & -2 \\ -2 & 1 & 0 & 1+a \\ 1+a & -2 & 1 & 0 \\ 0 & 1+a & -2 & 1 \end{bmatrix} \tag{2.27}$$

Note that this matrix becomes singular for $a = 0$ (the sum of the rows and columns is zero). In this case there is a double pole at $z = 1$.

The matrix $\boldsymbol{C}_4$ is:

$$\boldsymbol{C}_4 = \begin{bmatrix} 0 & 0 & b_2 - b_1 & b_1 \\ b_1 & 0 & 0 & b_2 - b_1 \\ b_2 - b_1 & b_1 & 0 & 0 \\ 0 & b_2 - b_1 & b_1 & 0 \end{bmatrix} \tag{2.28}$$

Let $b_1 = 1$, $b_2 = 0.5$ and $a = 0.1$. For zero modulator input, the periodic code sequence $\overline{10} = \overline{1010}$ gives $\boldsymbol{v} = [\ -1 \quad 1 \quad -1 \quad 1\ ]^\mathsf{T}$. Using Eq. (2.25), the steady-state filter output is $\boldsymbol{e} = [\ 0.366 \quad -0.366 \quad 0.366 \quad -0.366\ ]^\mathsf{T}$. The $\overline{10}$ limit cycle exists since $\mathrm{sgn}(e(n)) = y(n)$. This limit cycle is very persistent for most modulators and causes most modulators to have a tone at half the sample rate for zero input (see Ch. 8).

The periodic code sequence $\overline{1000}$ results in $\boldsymbol{e} = [\ 3.19 \quad 2.09 \quad 2.17 \quad 2.54\ ]^{\top}$; hence, this limit cycle does not exist for zero input. However, for a suitable negative constant modulator input, this limit cycle will exist: the dc-gain of $H(z)$ is 5; hence, for a constant dc-input in the interval $[-3.19/5, -2.54/5]$ the $\overline{1000}$ limit cycle exists □

2.8 Summary

This chapter has introduced Σ-Δ modulators as general discrete-time nonlinear dynamical systems. It was shown that the nonlinear dynamics of a modulator is only determined by the normalized feedback filter transfer function. Different modulator topologies sharing the same feedback filter are all equivalent when proper linear input filters are applied. Since linear filters are well known, it is only necessary to focus on the feedback filter inside the nonlinear loop around the quantizer.

The piecewise linearity of these systems simplifies the local stability analysis: the system behaves like a linear system in two disjoint domains and the poles of the feedback filters determine the local stability of fixed points and limit cycles. It was also demonstrated that the maps of Σ-Δ modulators have a noninvertible region where the map is two-to-one. Furthermore, it was shown that this region can be characterized generally from the quantizer input and the feedback filter transfer function evaluated at $z = 0$.

Finally, it was shown how the limit cycles of a modulator can be found by opening the loop. Furthermore, the output code sequences of a limit cycle is uniquely characterizing the corresponding orbit for most systems. Consequently, there is a one-to-one correspondence between limit cycles and the binary numbers.

Chapter 3

The Stability of Chaotic Σ-Δ Modulators

3.1 Introduction

The term 'stability' is often mentioned in connection with Σ-Δ modulators. Since a large number of stability definitions exist, a more explicit formulation of the stability of Σ-Δ modulators must be given. The practical problem is that a modulator operating with a given input suddenly might 'explode', i.e., the quantizer input starts oscillating with a rapidly increasing amplitude. These oscillations may become unbounded for the purely mathematical modulator described in Ch. 2; however, for real modulators, non-linearities such as arithmetic overflow and circuit saturation will limit the amplitude.

The onset of uncontrolled oscillations causes the signal encoding properties of the modulator to virtually disappear and the resulting signal-to-noise ratio decreases dramatically. Obviously, combinations of input signals and feedback filter parameters which cause instability should be avoided. The goal of the Σ-Δ modulator stability analysis is to answer the question: is a given modulator stable for a reasonably large set of initial conditions and with a given class of input signals?

This chapter focuses on the stability of chaotic modulators. The question in this case is: Does the system have a stable attractor and what is its basin of attraction?

It will appear from the numerous examples in this chapter that it is extremely difficult to derive an easily applied, general and not too conservative stability criterion.

Due to the usually high oversampling ratio, the input signals for real modulators will normally change slowly. In order to simplify the stability analysis, the input signal in the following is restricted to the class of constant input signals, i.e., the modulators can be described as an autonomous dynamical systems.

3.2 Chaotic Σ-Δ Modulators

When one or more poles of $H(z)$ are outside the unit circle, every fixed or periodic points is unstable; however, this does not necessarily mean that the orbits of the system become unbounded with time as it is the case for linear systems. Due to the possible existence of a non-invertible region U (see Sec. 2.6), the orbit may stay bounded. The reason for this is that the sets V_+ and V_- are both mapped on top of each other on the non-invertible region U. This folding mechanism seems to be necessary in order to bound the orbit in steady state. The existence of a folding mechanism in combination with state-space stretching, i.e., one or more eigenvalues are outside the unit circle, indicates the presence of chaos, i.e., the contracting effect of the folding mechanism counterbalances the state-space divergence. This motivates following assumption:

Assumption 3.1 *A Σ-Δ modulator with at least one $H(z)$ pole outside the unit circle and with a non-empty non-invertible region is assumed to be chaotic, i.e., a bounded limit set exists on which the modulator is chaotic. Furthermore, the intersection between the limit set and the non-invertible region is non-empty, i.e., the non-invertible set is visited repeatedly.*

3.3 Boundary Crisis

As stated in Section 3.1, the question of stability of chaotic modulators is: When is the chaotic limit set attracting and what is the corresponding basin of attraction? Generally, it is a very difficult task to answer this question, since the stability obviously depends on global properties rather than local stability analysis. To illustrate this: modulators can be made stable despite the fact that local state-space perturbations grow in all directions, i.e., all $H(z)$-poles are outside the unit circle. When a chaotic modulator is stable, a basin of attraction B_L with a non-zero measure exist, i.e., B_L is the set of initial conditions which are attracted asymptotically to the chaotic limit set. It is concluded from simulations that a chaotic modulator has at most one stable limit set which must chaotic since every limit cycle is unstable. Consequently, the initial conditions outside B_L will generally result in unbounded orbits; however, initial conditions which are exactly on other unstable limit points, e.g., points on limit cycles, will give bounded orbits which are not attracted to the chaotic limit. Therefore, unstable limit points not belonging to the chaotic attractor must either be on the boundary of B_L, ∂B_L or belong to the exterior of B_L. However, some of the limit points on the boundary of B_L can be points of accumulation of B_L, i.e., any sufficiently small non-zero perturbation gives an orbit which is attracted to the chaotic limit set. For limit points belonging to the exterior of B_L, any sufficiently small perturbation causes the orbit to become unbounded. Furthermore, ∂B_L must be invariant to the system map, i.e., every point on ∂B_L is mapped to another point on ∂B_L.

Obviously, an attracting chaotic limit set L must be contained in its corresponding basin of attraction, i.e., $L \subset B_L$. When the modulator input or filter parameters is changed such that the chaotic modulator becomes unstable, the basin of attraction B_L disappears. A way to interpret the onset of instability is to imagine that L 'grows' out of B_L or in general that L collides with the boundary of B_L. This type of bifurcation is often called a *boundary crisis* [22]. It is characteristic to this type of bifurcation that B_L suddenly disappears at the onset of instability rather than it gradually shrinks towards zero measure. Furthermore, the limit set does not 'jump' in size just before loosing stability. This explains why modulators may 'blow up' suddenly without any preceding warning.

Notice that after the onset of instability, a chaotic but unstable limit set survives. This means that there still exist initial conditions which give bounded orbits, namely the limit points; however, even small perturbations cause the modulator to 'blow up', i.e., the set of initial conditions giving bounded orbits has zero measure. Hence, the stability concept of a chaotic limit set is in good agreement with the practical modulator stability definition as defined in Section 3.1. In Section 3.5, the so-called escape rate will be defined which quantifies the instability of a repelling chaotic limit set.

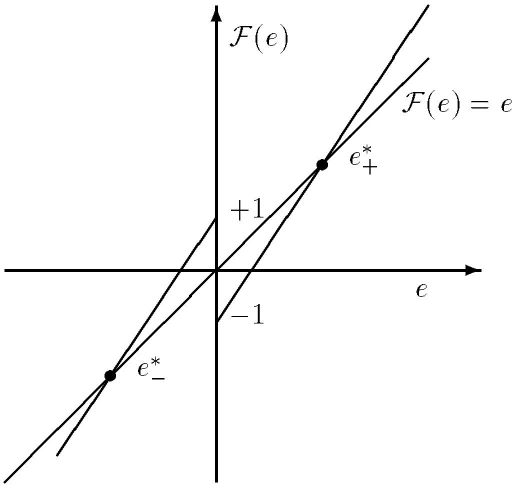

Figure 3.1: First order map $\mathcal{F}(e)$ according to Eq. (3.1) for zero input and $a > 1$.

Example 3.1 Consider the general first order Σ-Δ modulator with constant input given by the map:

$$e(n+1) = \mathcal{F}(e(n)) = ae(n) + i - \mathrm{sgn}(e(n)) \tag{3.1}$$

where i is the constant input and a is a parameter.

The map $\mathcal{F}$ is schematically shown in Fig. 3.1 for $a > 1$ and $i = 0$.

The corresponding feedback filter transfer function is:

$$H(z) = \frac{z^{-1}}{1 - az^{-1}} \tag{3.2}$$

The feedback filter has a pole at a. When a is less than unity, the map corresponds to a first order modulator with a leaky integrator [16, 45]. For $a = 1$, the system is equivalent to the well known circle map (rotation of the circle) [68] and this system is quasiperiodic for irrational constant input [15] . For $a > 1$ the modulator is generally chaotic [15], i.e., the pole at a is outside the unit circle.

Eq. (3.1) shows that for $a > 1$, the map has to fixed points given by:

$$\begin{aligned} e_+^* &= \frac{1-i}{a-1} \\ e_-^* &= \frac{-1-i}{a-1} \end{aligned} \tag{3.3}$$

The noninvertible set is the interval $U =]-1+i, 1+i[$ and the preimage of U is the interval $V =]2H(0), -2H(0)[=]\frac{-2}{a}, \frac{2}{a}[$.

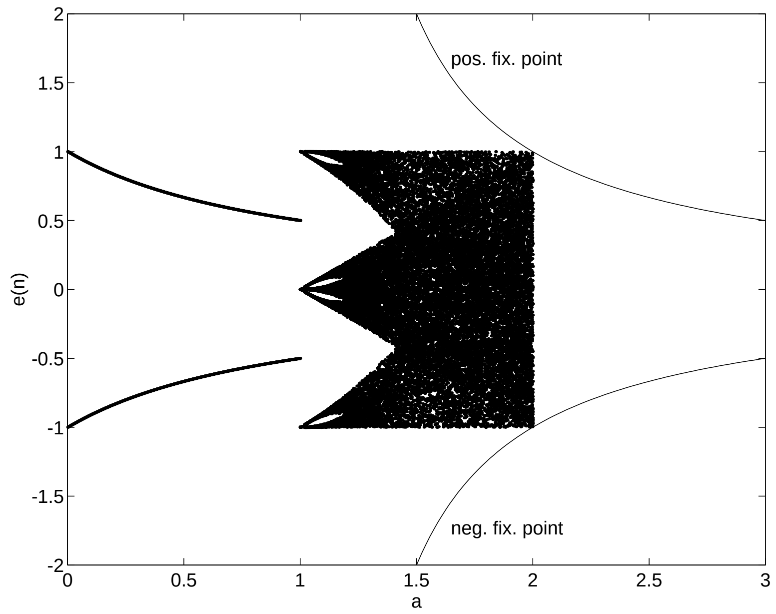

Figure 3.2: Bifurcation diagram of the first order modulator cf. Eq. (3.1) with zero input. The two hyperbolas are the loci of the two unstable fixed points for $a > 1$, cf. Eq. (3.3).

The unstable fixed points separate points which iterate to infinity from points which iterate towards the signum function threshold at $e = 0$. Points in a neighborhood of $e = 0$ are either mapped into a neighborhood of $e = 1 + i$ or $e = -1 + i$, i.e., the end-points of U. Consequently, the modulator is assumed to be stable if U is fully inside the interval between the unstable fixed points which is fulfilled when:

$$|i| < \frac{2}{a} - 1 \tag{3.4}$$

Hence, the stable input range decreases as a is increased.

When this condition is satisfied, the basin of attraction must be the interval between the unstable fixed points, i.e, $B_L =]e^*_-, e^*_+[$, and the chaotic limit set L must be contained in U, cf. Ass. 3.1.

Fig. 3.2 shows a bifurcation diagram for the first order modulator with zero input (see also [15, 59]). The modulator was simulated with a slowly increasing a-parameter and the obtained quantizer input $e(n)$ is plotted versus a. For $a < 1$, the stable $\overline{10}$ limit cycle is the only existing limit cycle (at most one limit cycle can exist at a time for fixed i and a for $a < 1$, cf. [15]). For $a > 1$, a chaotic limit set emerges including some more complex limit cycles like $\overline{1100}$. However, the now unstable $\overline{10}$ limit cycle is not included in the chaotic limit set. Notice that the chaotic limit set becomes unstable at $a = 2$ due to a collision with the unstable fixed points which form the boundary of B_L $\square$

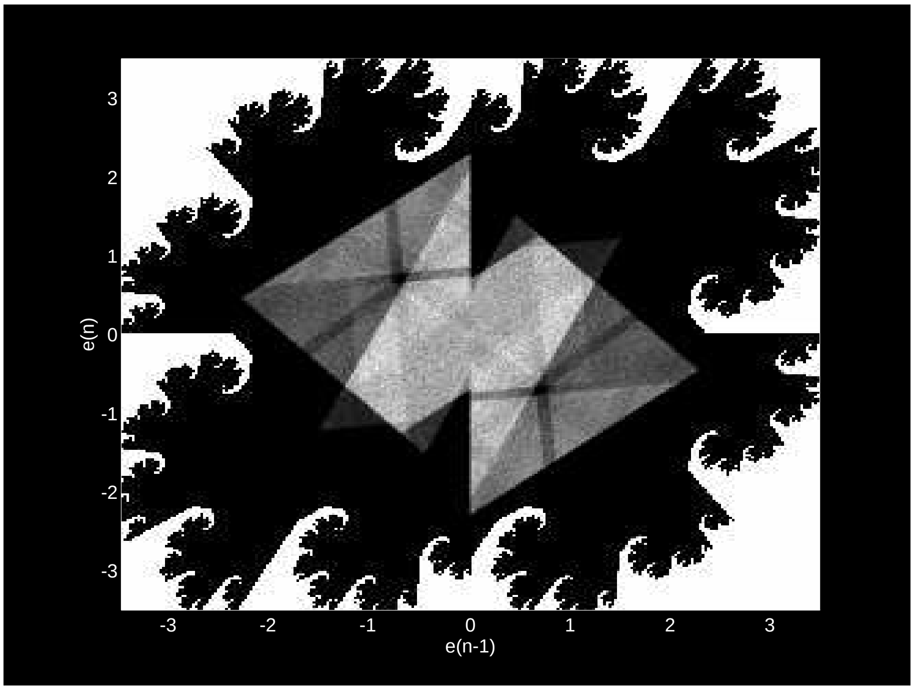

Figure 3.3: Basin of attraction B_L and limit set L for the modulator cf. Eq. (3.5) with $h_1 = 0.8$ and $h_2 = -1.5$.

3.4 Finding the Basin of Attraction

This section will focus on the onset of instability for chaotic modulators from a more practical point of view. Especially the often very complex structure of the chaotic limit set and the basin of attraction will be studied by simulations. The examples are based on second order modulators in order to enable graphical illustrations.

The basin of attraction, B_L of a modulator can in general not be determined analytically; hence, B_L must be estimated numerically. For all practical purposes, B_L is the set of initial conditions which give bounded orbits. The state-space must thus be sampled in a large number of grid points and the points giving orbits which stay bounded by a certain bound up to a certain maximum number of iterations, n_{max}, are marked as members of B_L. A stable chaotic limit set L can be approximated simply as the union of all points on an orbit starting within B_L; however, the initial transient of the orbit before steady state behavior is reached should be omitted.

Example 3.2 Fig. 3.3 and 3.4 shows B_L for two modulators with feedback filter

$$H(z) = \frac{h_1 z^{-1} + h_2 z^{-2}}{1 - h_1 z^{-1} - h_2 z^{-2}} \tag{3.5}$$

where h_1 is 0.8 and h_2 is -1.5 and -1.65.

This class of modulators has been investigated empirically as well as analytically in [60].

For each point in Fig. 3.3 and Fig. 3.4, up to 500 iterations were performed and points giving an quantizer input signal $|e(n)| < 10$ are plotted in black and

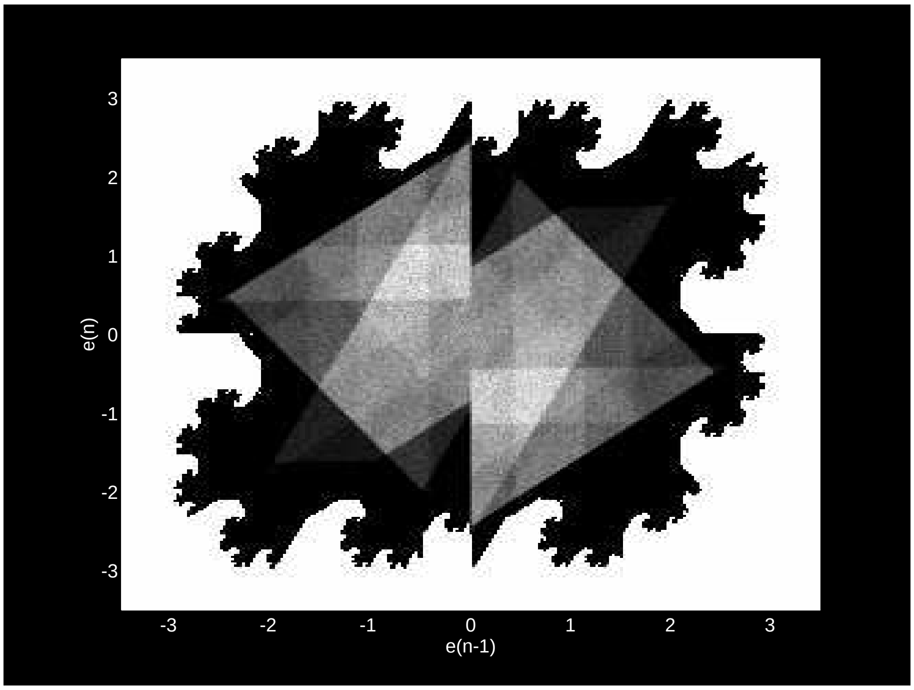

Figure 3.4: Basin of attraction B_L and limit set L for the modulator cf. Eq. (3.5) with $h_1 = 0.8$ and $h_2 = -1.65$.

the rest are white. The state-vector used is $\boldsymbol{x}_n = [e(n-1), e(n)]^\top$, i.e., the plots show the quantizer input $e(n)$ versus $e(n-1)$. In addition the stable chaotic limit sets are plotted using a gray scale; limit points which are frequently visited are lighter than limits points rarely visited. The figures indicate that both modulators are stable, but the space between the boundary of B_L and L reduces as h_2 is lowered to -1.65.

The modulator with $h_2 = -1.5$ was proven to be stable in [57]: it was shown that the regions of the state-space square with $|e| < 2$ which is mapped outside the square will return to the square again within a finite number of iterations, hence, this proves that the quantizer input is bounded. This approach works obviously only when the used square is fully inside B_L and this is not the case for $h_2 = -1.65$ (see Fig. 3.4).

When h_2 is approx. -1.7, L collides with ∂B_L and the modulator becomes unstable. This can be observed from Fig. 3.5 and Fig. 3.6 for $h_2 = 1.8$ where B_L has been estimated using n_{max} equal to 100 and 500. Observe that the estimated B_L sets becomes 'thinner' for higher n_{max}, i.e., the number of grid points surviving (i.e., staying below a bound) n_{max} iterations decreases with n_{max} $\square$

3.5 The Escape Rate

The observations done in Example 3.2 inspire to the assumption that a certain fraction of orbits stemming from random initial conditions will not survive the $(k+1)$'th iteration for an unstable system. Consequently, it is assumed that the number of survivors decreases exponentially with k [13] and thereby the so-called *escape rate* γ is defined:

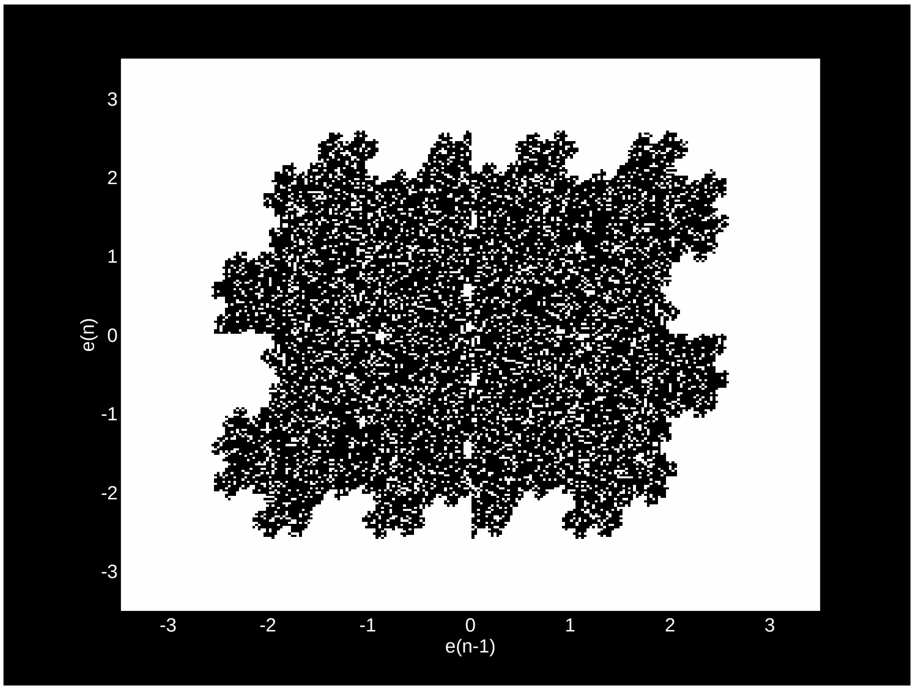

Figure 3.5: Estimate of the basin of attraction B_L for the modulator cf. Eq. (3.5) with $h_1 = 0.8$, $h_2 = -1.8$ and maximum iteration number $n_{max} = 100$.

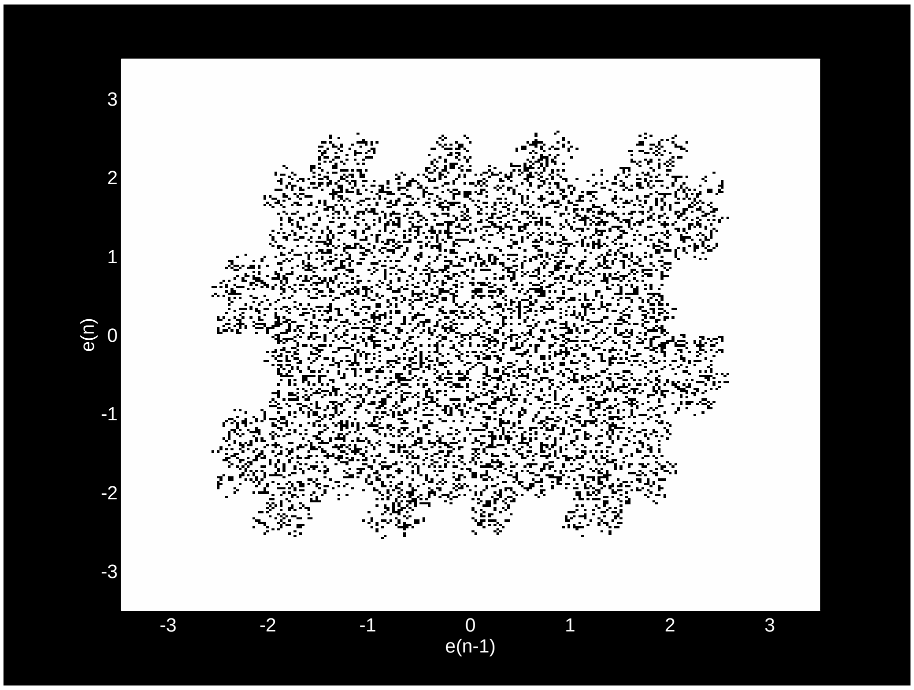

Figure 3.6: Estimate of the basin of attraction B_L for the modulator cf. Eq. (3.5) with $h_1 = 0.8$, $h_2 = -1.8$ and maximum iteration number $n_{max} = 500$.

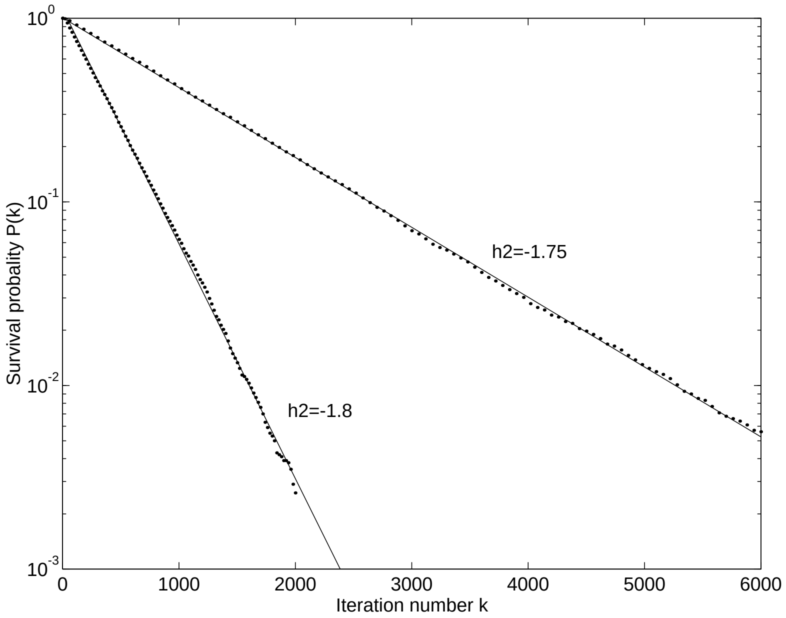

Figure 3.7: Survival probability $P(k)$ as a function of the iteration number k.

Assumption 3.2 *The probability $P(k)$ that the orbit of an unstable chaotic modulator with random initial condition stays inside a suitable bounding set W for k iterations is assumed to be:*

$$P(k) = \Pr\{\forall_{n \le k} : \boldsymbol{x}_n \in W\} = P_0\, e^{-\gamma k} \tag{3.6}$$

where P_0 depends on the probability distribution of initial conditions $\boldsymbol{x}_0$ and γ is the escape rate. The mean survival time is defined as $T = 1/\gamma$.

In order to give a meaningful escape rate, the unstable repeller must be contained in the bounding set W used in Eq. (3.6). When an orbit leaves this set, the orbit should never return into W again, i.e., every point outside W should escape to infinity or another attractor. In Example 3.2 the bounding set W was the set of state-vectors with quantizer input magnitude less than some maximum value. When P_0 is unity, then the mean survival time $T = 1/\gamma$ is the average number of time steps the system 'lives' before it escapes. Generally P_0 is the fraction of initial points that do not escape within the first time steps. If the distribution of initial points covers far more than the limit set then P_0 will be small and it will take some time steps before the orbits starts to escape. The assumed exponential decay of $P(k)$ is thus only accurate for large k.

The existence of an escape-rate necessitates that the bounding set W contains a number of limit cycles or fixed points, i.e., for suitably chosen initial conditions, it is possible to stay forever inside W. This condition is normally fulfilled, since a chaotic limit set has infinitely many limit cycles.

The exponential decay is similar to the decay of radioactive material.

Example 3.3 The exponential decay of survivors, can be investigated numerically. The system is simulated with a large number of suitably distributed random initial conditions and the iteration number for which the system exceeds a given bound is estimated. Subsequently, the fraction of survivors are plotted on log-scale versus the iteration number on lin-scale yielding a straight line with slope equal to the escape rate. Fig. 3.7 shows this type of plot for the second order modulator cf. Eq. (3.5) for $h_1 = 0.8$. Two plots are shown: $h_2 = -1.75$ giving $\gamma = 8.8 \cdot 10^{-4}$ and $h_2 = -1.8$ giving $\gamma = 2.9 \cdot 10^{-3}$. Both plots are based on 10.000 random initial conditions and the orbits are considered as survivors until the quantizer input magnitude exceeds 10. The asymptotic slope of the survival plots (i.e., the escape rate) does naturally not depend on the choice of bounding set as long as the repeller is fully included herein $\square$

3.6 The Structure of L and B_L

Generally, the shapes of the stable limit set L and the basin of attraction B_L are very complicated and impossible to describe analytically except for a very few cases (like Example 3.1). This makes it almost impossible to find a comprehensive analytical stability criterion for the general class of modulators. In the following a number of examples will demonstrate the complexity of especially the basin of attraction.

The next example demonstrates that a certain subset of second order modulators have a very simple B_L set which can be described analytically and in addition, the chaotic limit set can be bounded to a certain region. This fact allows the derivation of a sufficient stability criterion.

Example 3.4 Consider the second order multiple feedback modulator discussed in Example 2.3 (see Fig. 2.6) with constant input i. In order to normalize the feedback transfer function $H(z)$, the parameter b_1 is set to unity and the parameter b_2 is substituted for b. This normalization reflects the fact that there is only one degree of freedom for the choice of the zero of $H(z)$. The multiple feedback modulator is equivalent to an usual Σ-Δ modulator preceded filtered by a prefilter. The prefilter has in this case the following first order transfer function, cf. Eq. (2.14):

$$G(z)H^{-1}(z) = \frac{z^{-1}}{1 + (b-1)z^{-1}} \tag{3.7}$$

Since only constant input is considered, the prefilter scales the input by factor $1/b$. Consequently, scaling of the input for the multiple feedback modulator by a factor b makes the multiple feedback modulator equivalent to a usual Σ-Δ modulator for constant input. Using this scaling, the system can be characterized by the following map:

$$\boldsymbol{x}_{n+1} = \mathcal{F}(\boldsymbol{x}_n) = \begin{bmatrix} 1 & 1 \\ -a & 1 \end{bmatrix} \boldsymbol{x}_n - \mathrm{sgn}\left(\begin{bmatrix} 1 & 0 \end{bmatrix} \boldsymbol{x}_n \right) \begin{bmatrix} 1 \\ b \end{bmatrix} + \begin{bmatrix} 0 \\ bi \end{bmatrix} \tag{3.8}$$

The state vector is given by $\boldsymbol{x}_n = \begin{bmatrix} x_1(n) & x_2(n) \end{bmatrix}^\top$ where $x_1(n)$ is the quantizer input.

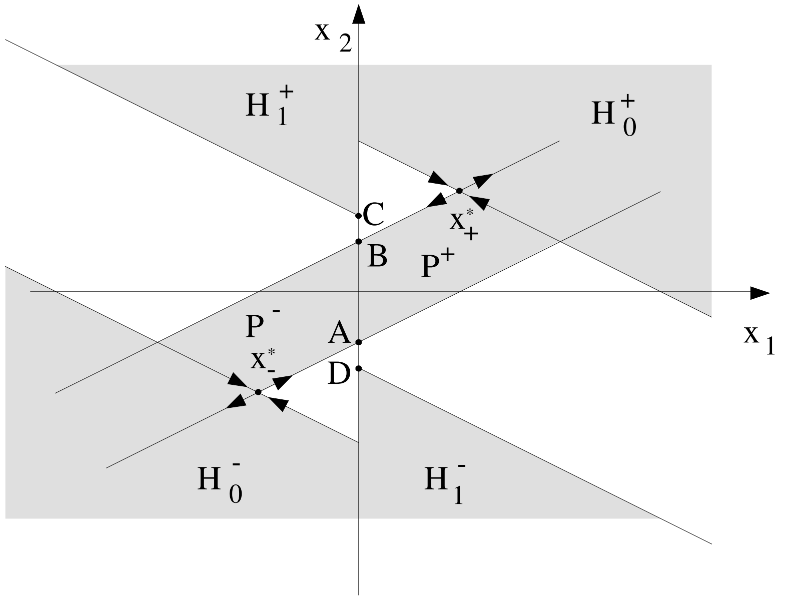

Figure 3.8: The geometry of the multiple feedback modulator from Example 3.4 for $a < 0$ and $b < \sqrt{-a}$.

For negative a, the system has two fixed points:

$$\boldsymbol{x}_{+}^{*} = \begin{bmatrix} \frac{b(1-i)}{-a} \\ 1 \end{bmatrix}, \boldsymbol{x}_{-}^{*} = \begin{bmatrix} \frac{-b(1+i)}{-a} \\ 1 \end{bmatrix} \tag{3.9}$$

The system has the eigenvalues or poles of $H(z)$:

$$z = 1 \pm \sqrt{-a} \tag{3.10}$$

For $-4 < a < 0$ there are two real valued eigenvalues; one outside and one inside the unit circle. Consequently, each of the two fixed points are *saddle points* and they have a stable and an unstable manifold [46]. The manifolds are just straight lines in the eigenvector directions and the manifolds are invariant to the system map. The stable manifold of $\boldsymbol{x}_{+}^{*}$ corresponding to the eigenvalue $z = 1 - \sqrt{-a}$ is given by:

$$\begin{aligned} \mathcal{F}(\boldsymbol{x} - \boldsymbol{x}_{+}^{*}) &= (1-\sqrt{-a})(\boldsymbol{x} - \boldsymbol{x}_{+}^{*}) \Leftrightarrow \\ \left(\begin{bmatrix} 1 & 1 \\ -a & 1 \end{bmatrix} - (1-\sqrt{-a})\boldsymbol{E} \right) \boldsymbol{x} &= \left(\begin{bmatrix} 1 & 1 \\ -a & 1 \end{bmatrix} - (1-\sqrt{-a})\boldsymbol{E} \right) \boldsymbol{x}_{+}^{*} \Leftrightarrow \\ \begin{bmatrix} \sqrt{-a} & 1 \end{bmatrix} \boldsymbol{x} &= \frac{b(1-i)}{\sqrt{-a}} + 1 \end{aligned} \tag{3.11}$$

Similarly, the unstable manifold of $\boldsymbol{x}_{+}^{*}$ corresponding to the eigenvalue $1 + \sqrt{-a}$ is given by:

$$\begin{bmatrix} -\sqrt{-a} & 1 \end{bmatrix} \boldsymbol{x} = \frac{-b(1-i)}{\sqrt{-a}} + 1 \tag{3.12}$$

The stable manifold of $\boldsymbol{x}_+^*$ separates points with $x_1 > 0$ which iterate towards infinity from points which iterate towards the quantizer threshold at $x_1 = 0$. The geometry is shown in Fig. 3.8 for $b < \sqrt{-a}$ where the shaded area H_0^+ is the points which escape to infinity along the unstable manifold. Similarly, the stable manifold of $\boldsymbol{x}_-^*$ delimits the shaded area H_0^- of points with $x_1 < 0$ iterating towards infinity. Consequently, both fixed points and parts of their stable manifolds are on the boundary of B_L if the system is stable. The shaded set H_1^+ is the preimage of H_0^+ with respect to $\mathcal{F}_-$, i.e., $H_1^+ = \mathcal{F}_-^{-1}(H_0^+)$; furthermore, this set must be fully outside B_L for the same reasons as for H_0^+. the wedge H_1^+ is delimited by the line $x_1 = 0$ and by a line parallel to the stable manifold of $\boldsymbol{x}_+^*$ which intersects the line $x_1 = 0$ at the point $\mathrm{C} = [\ 0 \quad x_{2,c}\ ]^\top$ in Fig. 3.8. Furthermore, it can be concluded that the point C must be on ∂B_L since any neighborhood of C is mapped on both sides of the stable manifold of $\boldsymbol{x}_+^*$. The point C can be found from the condition that $\mathcal{F}_-(C)$ must be on the stable manifold of $\boldsymbol{x}_+^*$. Using Eq. (3.11) one arrives at:

$$\begin{array}{c} \left[\ \sqrt{-a} \quad 1\ \right] \mathcal{F}_-\left(\left[\begin{array}{c} 0 \\ x_{2,c} \end{array}\right]\right) = \frac{b(1-i)}{\sqrt{-a}} + 1 \ \Leftrightarrow \\ \sqrt{-a}(x_{2,c}+1) + x_{2,c} + b(1+i) = \frac{b(1-i)}{\sqrt{-a}} + 1 \ \Leftrightarrow \\ x_{2,c} = \frac{1}{1+\sqrt{-a}}\left(\frac{b(1-i)}{\sqrt{-a}} + 1 - b(1+i) - \sqrt{-a}\right) \end{array} \tag{3.13}$$

Similarly, the shaded region H_1^- in Fig. 3.8 is the preimage of H_0^- with respect to $\mathcal{F}_+$ and the region is a wedge characterized the point D which like C is on ∂B_L.

The hatched region $\mathrm{P} = \mathrm{P}^+ \bigcup \mathrm{P}^-$ in Fig. 3.8 is delimited by all the four manifolds. The chaotic limit set L must be inside P since points outside the stable manifolds iterate to infinity and points just outside the unstable manifolds but inside the stable manifolds must iterate into P. Consequently, a sufficient but not necessary stability criterion is that the modulator is stable when the set P does not collide with the boundary of B_L, i.e., when P is a so-called *trapping region* which is mapped into it self. This condition holds when the both the points C and D on ∂B_L are outside P for $b < \sqrt{-a}$. The reason is that orbits escaping the system from an initial point inside P must sooner or later enter H_1^- or H_1^+ before the orbit escapes along one of the unstable manifolds and C and D will be the first points in these sets which will be hit at a collision between L and B_L. For positive input and $b < \sqrt{-a}$ the criterion is fulfilled as long as the point C does not cross the unstable manifold of $\boldsymbol{x}_+^*$. Using Eq. (3.12) and Eq. (3.13) the stability criterion holds for positive input i when:

$$\begin{array}{c} \left[\ -\sqrt{-a} \quad 1\ \right]\left[\begin{array}{c} 0 \\ x_{2,c} \end{array}\right] > \frac{-b(1-i)}{\sqrt{-a}} + 1 \ \Leftrightarrow \\ \frac{1}{1+\sqrt{-a}}\left(\frac{b(1-i)}{\sqrt{-a}} + 1 - b(1+i) - \sqrt{-a}\right) > \frac{-b(1-i)}{\sqrt{-a}} + 1 \ \Leftrightarrow \\ i < \frac{a+b}{b(1+\sqrt{-a})}\ ,\ \text{for } i > 0\ ,\ b < \sqrt{-a} \end{array} \tag{3.14}$$

Due to the symmetry of the system, the sufficient stability criterion can be extended to:

$$|i| < \frac{a+b}{b(1+\sqrt{-a})}\ ,\ b < \sqrt{-a} \tag{3.15}$$

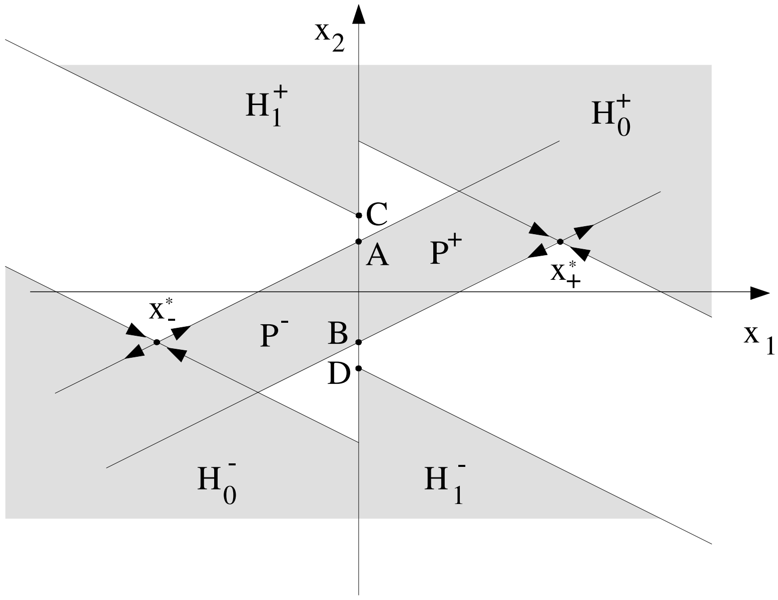

Figure 3.9: The geometry of the multiple feedback modulator from Example 3.4 for $a < 0$ and $b > \sqrt{-a}$.

For $b = \sqrt{-a}$ an interesting situation arises: the unstable manifolds of the two fixed points become identical and the set P is thus the line segment between the fixed points and P is identical to B_L. Consequently, the chaotic limit set L of the two dimensional system is embedded in a one dimensional subspace and the dynamics of the system can thus asymptotically be described by a one dimensional map. This phenomenon is also reflected by the feedback transfer function $H(z)$ from Eq. (2.11):

$$H(z) = \frac{z^{-1}\left(1-(1-b)z^{-1}\right)}{(1-(1+\sqrt{-a})z^{-1})(1-(1-\sqrt{-a})z^{-1})} \tag{3.16}$$

which shows that a real pole at $1-\sqrt{-a}$ and a real zero at $1-b$ are cancelling for $b = \sqrt{-a}$, i.e., the system is a first order modulator embedded in a second-order system. The same situation occurs for $b = -\sqrt{-a}$, but in this case, the resulting non-chaotic first order modulator is unstable due to the embedding into a diverging state-space.

The geometry of the system is shown for $b > \sqrt{-a}$ in Fig. 3.9; the set P is two-dimensional again. For this case and for positive input, the point C must not cross the unstable manifold of $\boldsymbol{x}_-^*$ in order to meet the sufficient stability criterion. Using the symmetry, Eq. (3.13) and an equation for the unstable manifold of $\boldsymbol{x}_-^*$ the criterion becomes:

$$\begin{gathered}
\begin{bmatrix} -\sqrt{-a} & 1 \end{bmatrix} \begin{bmatrix} 0 \\ x_{2,c} \end{bmatrix} > \frac{b(1+|i|)}{\sqrt{-a}} - 1 \Leftrightarrow \\
\frac{1}{1+\sqrt{-a}}\left(\frac{b(1-|i|)}{\sqrt{-a}} + 1 - b(1+|i|) - \sqrt{-a}\right) > \frac{b(1+|i|)}{\sqrt{-a}} - 1 \Leftrightarrow \\
|i| < \frac{1/b-1}{1+1/\sqrt{-a}}\,,\ b > \sqrt{-a}
\end{gathered} \tag{3.17}$$

The sufficient stability criteria of Eq. (3.15) and Eq. (3.17) indicate the maximum stable constant input amplitude as a function of the modulator parameters a and b. Numerical stability analysis will validate these criteria in Example 3.10 and it will appear that the criteria can be somewhat pessimistic for some parameter values. An improved stability criterion for $b > \sqrt{-a}$ has been made in [50]. This criterion is based on a more detailed (and complex) geometric analysis □

This example allowed an analytical study primarily due to the fact that the eigenvalues were both real and one was inside the unit circle. This kind of stability analysis is very difficult to perform on general high-order modulators. Even the general second-order modulator with complex poles is virtually impossible to analyze. The traditional double-loop modulator (i.e., a second-order modulator with two poles at $z = 1$) has been investigated intensively and rigorous stability criteria have been made [67, 47, 25].

3.7 Reverse Time Simulation

When all eigenvalues are complex and outside the unit circle, the analysis gets extremely complex. The basins of attraction shown in Fig. 3.3 and 3.4 correspond to modulators of this category and the basins of attraction have indeed a very complex structure. A closer analysis shows that the basin boundaries contain a large number of limit cycles and seem to be fractal. This fact indicates that an unstable chaotic limit set or repeller exists on ∂B_L simultaneously with the stable chaotic limit set L.

Normally it is almost impossible to locate a chaotic repeller numerically; however, in this particular case a reversal of the time axis can solve the problem. When a system with all eigenvalues outside the unit circle is iterated in reverse time, all limit cycles become attracting. As mentioned in Ch. 2, the map of a Σ-Δ modulator is noninvertible in a certain region U where two solutions exist. Consequently, reverse time simulation is generally a traversal of a binary tree where each time step is a node with a corresponding point in the state-space.

When a node is in U, there will be two branches from the node corresponding to the two inverse map solutions. Every node in the tree corresponds thus to points in state-space which ends on the initial node in forward time. Some of the branches in the tree can be the beginning of a path which never enters U, i.e., there is only one branch on each of the succeeding nodes. These paths are attracted to a limit cycle which is fully outside U. For some modulators, there are no such limit cycles and almost every branch will sooner or later lead to a node in U with two branches again leading to nodes in U. In these cases a chaotic repeller exists which is attracting in reverse time. Consequently, when a path in the tree, which repeatedly enters U, is followed, the state-space points corresponding to the nodes of the path will get closer and closer to the repeller. Picking the branches randomly, the entire repeller can be sampled and plotted graphically. Empirically, this procedure has proven to work irrespectively of the initial point (i.e., the initial node). This seems to indicate that the forward time system can reach any point in the state-space using initial conditions arbitrarily close to the repeller.

Example 3.5 Fig. 3.10 demonstrates an example of reverse time simulation using random branches of the stable modulator used for Fig. 3.3 (i.e., feedback

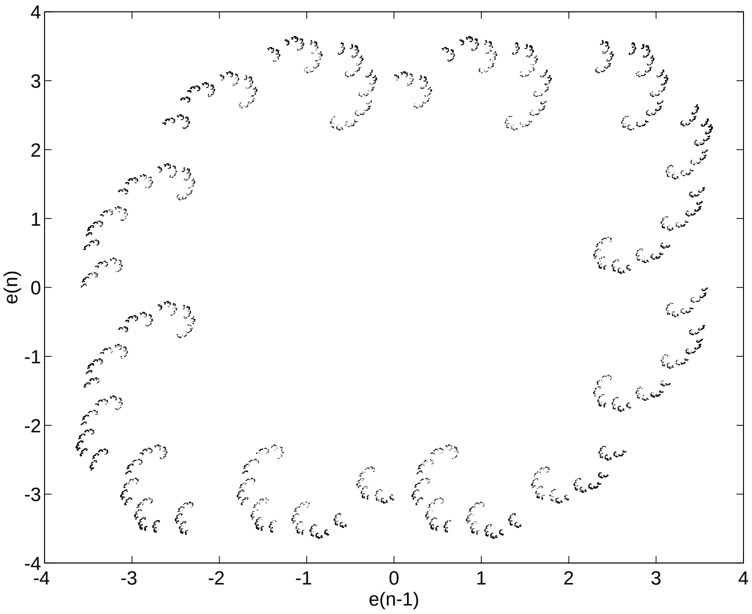

Figure 3.10: Reverse time simulation revealing the chaotic repeller of a stable modulator cf. Eq. (3.5) with $h_1 = 0.8$ and $h_2 = -1.5$. Compare the plot to Fig. 3.3.

filter cf. Eq. (3.5) with $h_1 = 0.8$ and $h_2 = -1.5$). A total of 30.000 points are plotted revealing a very complicated fractal set which fits the boundary of B_L shown in Fig. 3.3; however, this time reverse plot shows much more details □

A chaotic repeller is normally not observable since only orbits with initial conditions exactly on the repeller itself will follow the repeller. Orbits starting close to the repeller will either escape to infinity or be attracted to possible stable limit sets. In the former example the repeller lives on the boundary of the basin of attraction for a stable chaotic limit set, i.e., points close to the repeller are either escaping or being attracted to the stable chaotic limit set. The repulsion from the boundary repeller is forming a kind of 'embankment' around the stable limit set which keeps the stable limit set together: points on the inner side of the embankment stays inside and points on the outside are escaping. Whereas ∂B_L is simple in a one-dimensional system (see Example 3.1), the geometry gets more and more complex for higher order systems.

The degree on instability of a repeller on ∂B_L can, as for other unstable limit sets, be quantified, i.e., an escape rate can be found.

Example 3.6 The escape rate of the repeller shown in Fig. 3.10 can be measured by simulations when a suitable bounding set W is defined. Let W be the set of state-space points satisfying $(2 < |e(n)| < 4) \wedge (2 < |e(n-1)| < 4)$. The stable chaotic limit set is almost fully outside this set while the repeller in fully inside (see also Fig. 3.3). The survival probability $P(k)$ was measured versus the iteration number k using simulations with random initial conditions and the result was plotted in Fig. 3.12. The graph shows an almost straight

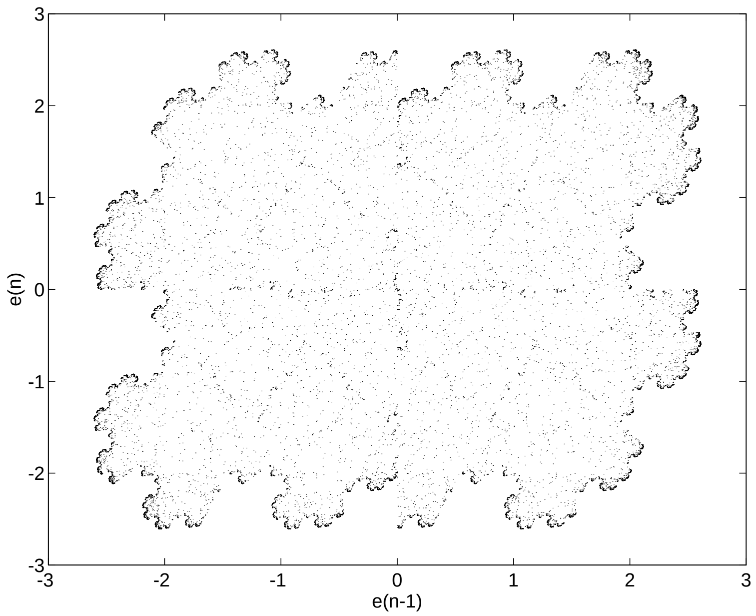

Figure 3.11: Reverse time simulation revealing the chaotic repeller of an unstable modulator cf. Eq. (3.5) with $h_1 = 0.8$ and $h_2 = -1.8$.

line with a slope corresponding to an escape rate of 0.175 equivalent to a mean survival time of approx. 6 time steps. This is indeed a very unstable repeller $\square$

As demonstrated previously, the modulator cf. Eq. (3.5) becomes unstable when h_2 is lowered to approx. -1.7 for $h_1 = 0.8$. At this point, the stable chaotic limit set L collides with the boundary of the basin of attraction which contains a chaotic repeller. During this collision, the chaotic repeller absorbs the formerly stable chaotic limit set leaving only a chaotic repeller. This repeller can again be seen using reverse time simulation for this type of collision between a stable and unstable chaotic limit set.

Example 3.7 Fig. 3.11 shows a reverse time simulation of the unstable modulator cf. Eq. (3.5) with $h_1 = 0.8$ and $h_2 = -1.8$. The plot reveals the chaotic repeller $\square$

It is only a subset of the Σ-Δ modulators which has a chaotic repeller living at the boundary of the basin of attraction. For some parameter values, a reverse time simulation using random branches is always attracted to a dominating limit cycle with no points in the noninvertible region U (such limit cycles will trap the system in reverse time). In principle, a reverse time simulation can get arbitrarily close to any limit cycle, if certain branches are deliberately used. However, when random branches are used, the reverse time system will asymptotically be trapped by a limit cycle totally outside U or be attracted to a chaotic repeller consisting of infinitely many limit cycles with orbits entering U. In fact, simulations seem to indicate that the asymptotic behavior of the reverse time system using

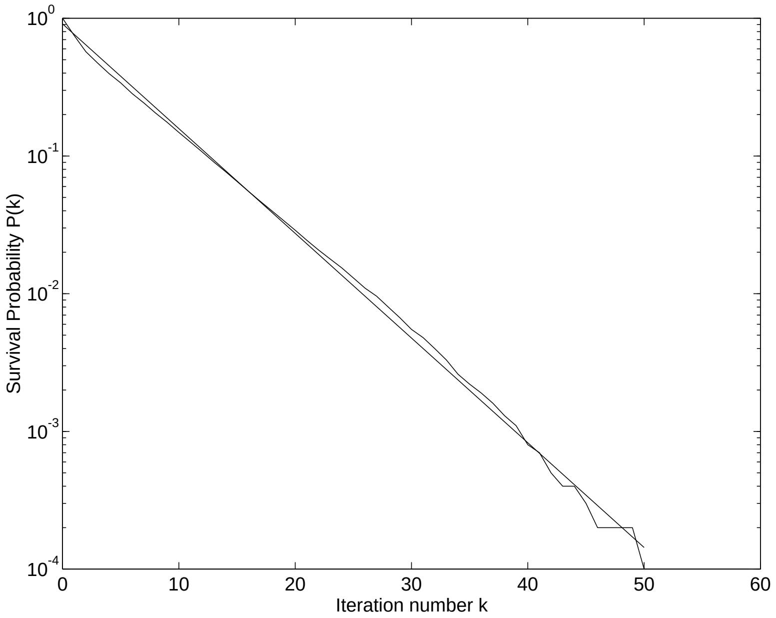

Figure 3.12: Survival probability $P(k)$ vs. iteration number k for the chaotic repeller on ∂B_L for the modulator cf. Eq. (3.5) with $h_1 = 0.8$ and $h_2 = -1.5$. The plot indicates an escape rate $\gamma = 0.175$.

random branches often is independent of the initial condition. In this case, the reverse time system is attracted to points which by means of an arbitrarily small perturbation can hit any place in the entire state-space in forward time. Such points must obviously belong to ∂B_L.

Typically, a modulator has a dominating limit cycle outside U corresponding to a periodic output signal having p positive codes followed by p negative codes which is called a $(\overline{p,p})$ limit cycle. Imagine that the modulator also has a $(\overline{p+1,p+1})$ limit cycle with an orbit entering U. The $(\overline{p+1,p+1})$ limit cycle cannot attract the reverse time system unless certain branches a used for each time step; hence, when random branches are used, it is almost certain that the system is trapped by the $(\overline{p,p})$ limit cycle. In some situations, the modulator parameters can be perturbed such that both the orbits of the dominant $(\overline{p,p})$ limit cycle and the $(\overline{p+1,p+1})$ limit cycle enter U at the same time, and at this point, a chaotic repeller might arise. This can be explained as follows: when the $(\overline{p,p})$ cycle is followed in reverse time, a $(p, p+1)$ code segment might be generated when a 'wrong' branch is used at a point in U. When the system later enters U again, two branches can be taken. The result is that the reverse time system repeatedly enters U and will produce a random output code sequence composed of the four segments (p, p), $(p, p+1)$, $(p+1, p)$ and $(p+1, p+1)$. The reverse time system is no longer attracted to a single limit cycle but to a chaotic limit set or repeller which consists of infinitely many 'hybrid' limit cycles composed of the previously mentioned four segments.

Large parts of the stable and chaotic parameter space for the second order modulator cf. Eq. (3.5) show a diversity of beautiful chaotic repellers coexisting with the stable (forward) chaotic limit set.

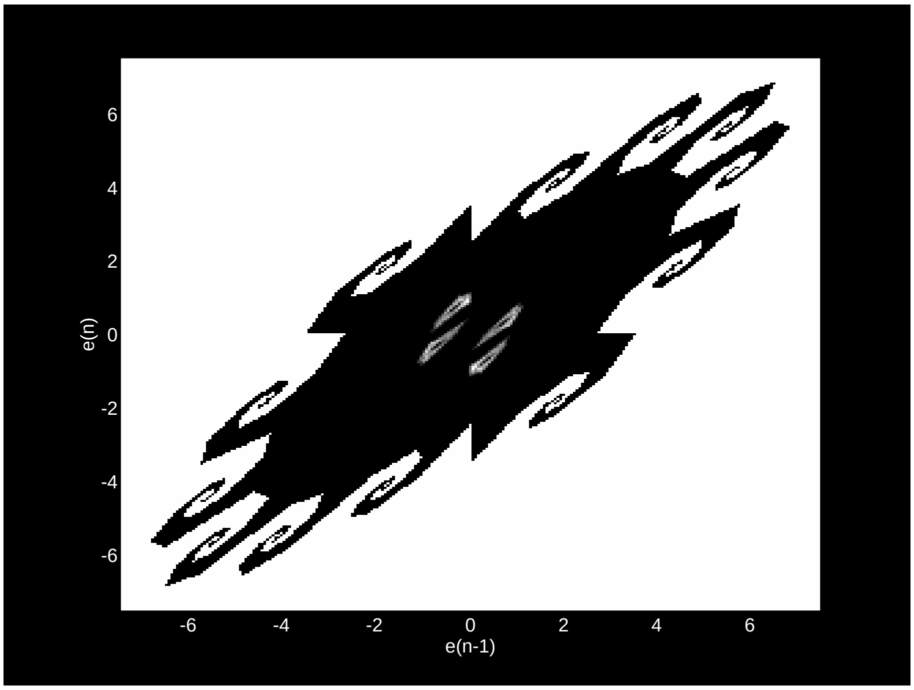

Figure 3.13: Basin of attraction and limit set for the modulator cf. Eq. (3.18) with zero input and $b = 0.45$.

Example 3.8 Consider the modulator with feedback filter

$$H(z) = \frac{z^{-1} - bz^{-2}}{1 - 1.95z^{-1} + 1.1z^{-2}} \tag{3.18}$$

with complex poles outside the unit circle. For $b = 0.45$ and zero input the system is stable and has $(\overline{p,p})$ limit cycles for $p = 1, 2, 3, 4, 5, 6$. Only the $(\overline{6,6})$ limit cycle is totally outside U. This can be observed from the corresponding periodic quantizer input signal $e(n)$ which is the repeated sequence $\langle$1.8 4.2 5.5 5.7 4.4 1.8 -1.8 -4.2 -5.5 -5.7 -4.4 -1.8$\rangle$. Recall from Eq. (2.19) that modulator states with quantizer input satisfying $|e| < -2H(z = 0)$ are in the set V which is mapped into U. Consequently, the $(\overline{6,6})$ limit cycle does not enter U since $\min(|e(n)|) > -2H(z = 0) = 2b/1.1 \approx 0.82$ and the reverse time system is thus asymptotically attracted to this limit cycle. All the other $(\overline{p,p})$ limit cycles enter U. Fig. 3.13 shows the basin of attraction for the modulator including the stable (forward) limit set. As expected, the $(\overline{6,6})$ limit cycle is on the boundary of B_L which forms a spiral around all the points on the limit cycle. Fig. 3.14 is a magnified plot around one of the points on the limit cycle and this plot shows clearly that B_L seems to spiral infinitely many times around the centers.

A (7,7) limit cycle arises when b is increased to 0.5. This limit cycle enters U and the system is thus still attracted to the (6,6) limit cycle in reverse time. Fig. 3.15 shows the basin of attraction and the limit set for $b = 0.5$. Notice that the spirals around the (6,6) limit cycle are preserved but the shape of

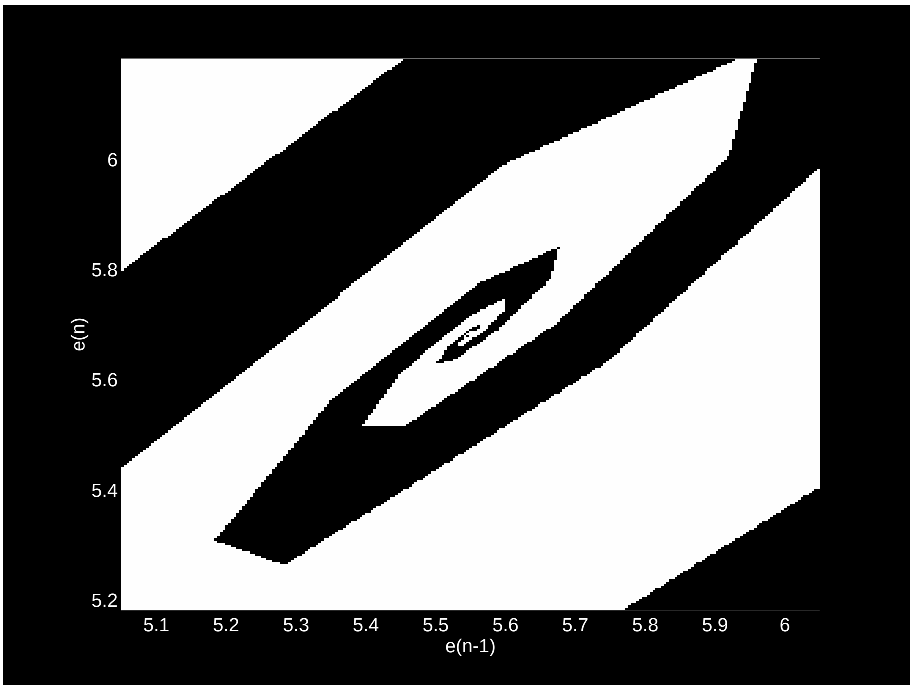

Figure 3.14: Magnified plot of the basin of attraction shown in Fig. 3.13 The center of the spiral is a point on the $(\overline{6,6})$ limit cycle.

B_L has become more complicated than for $b = 0.45$. This is probably due the onset of the (7,7) limit cycle outside B_L which is plotted with circles.

When b is increased to 0.56, both the $(\overline{6,6})$ and the $(\overline{7,7})$ limit cycles enter U which indicates the presence of a chaotic repeller on ∂B_L. This is indeed confirmed by Fig. 3.16 which is a plot of a reverse time simulation revealing a complex fractal set located in the space 'between' the $(\overline{6,6})$ and $(\overline{7,7})$ limit cycles which are shown with circles and crosses. Orbits close to this repeller will produce an output code composed of the segments $(6,6)$, $(6,7)$ $(7,6)$ and $(7,7)$.

Around $b = 0.58$ the $(\overline{7,7})$ limit cycle is totally outside U and the chaotic repeller disappears. Now the reverse time system is attracted to the $(\overline{7,7})$ limit cycle.

The bifurcations of the $(\overline{p,p})$ limit cycles can be observed in Fig. 3.17 which shows the minimum quantizer input magnitudes as a function of b. The straight dashed line shows the V-interval limit at $-2H(z=0) = 2b/1.1$. The plot shows clearly the succession of dominant $(\overline{p,p})$ limit cycles outside U and the windows for which there exist a chaotic repeller when no $(\overline{p,p})$ limit cycle is outside U. Many of the conclusions drawn from this example can be seen from the bifurcation diagram: the small window with a chaotic repeller around $b = 0.56$ (Fig. 3.16) surrounded by regions where either the $(\overline{6,6})$ or the $(\overline{7,7})$ limit cycle is outside U and on ∂B_L.

The very nice basin of attraction seen for $b = 0.45$ is at a region where the dominant $(\overline{6,6})$ limit cycle is peaking while no other limit cycles are outside U. At slightly lower b values, both the $(\overline{5,5})$ and $(\overline{6,6})$ limit cycles are outside U and this situation will be analyzed in detail later in Example 3.9. Fig. 3.17

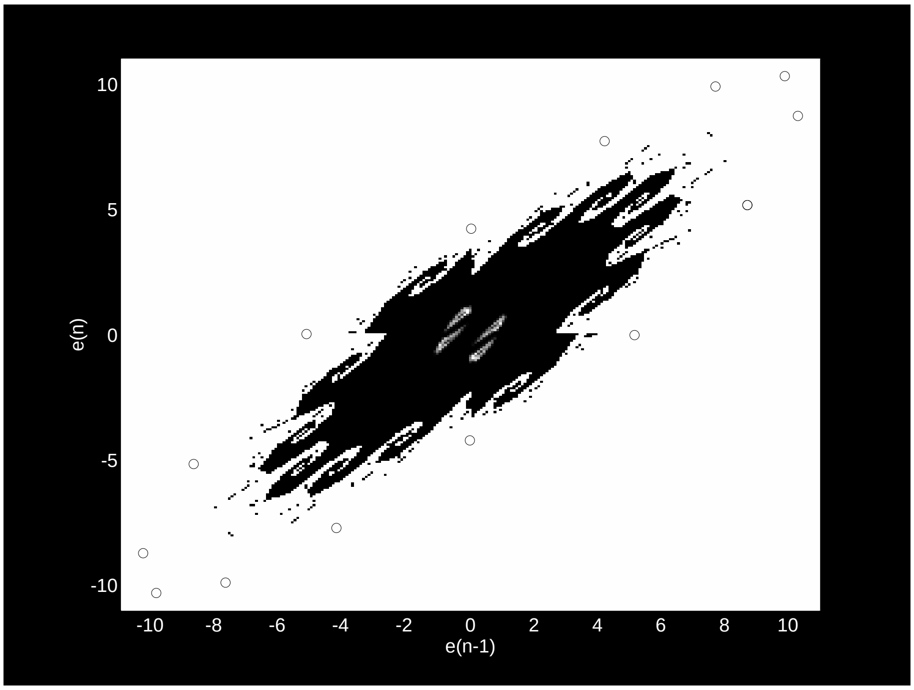

Figure 3.15: Basin of attraction and limit set for the modulator cf. Eq. (3.18) with zero input and $b = 0.5$. The $(\overline{7,7})$ limit cycle is plotted with circles.

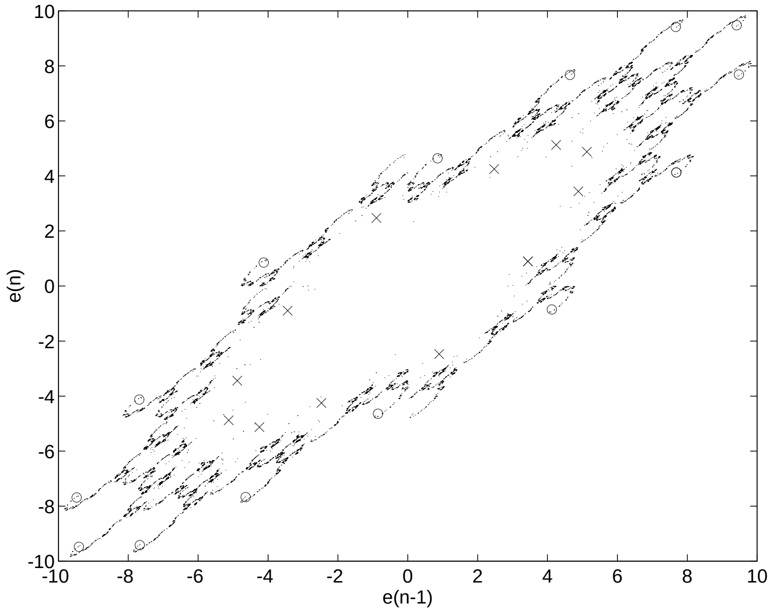

Figure 3.16: Reverse time simulation of the modulator cf. Eq. (3.18) with zero input and $b = 0.56$. The (6,6) and (7,7) limit cycles are plotted with crosses and circles, respectively.

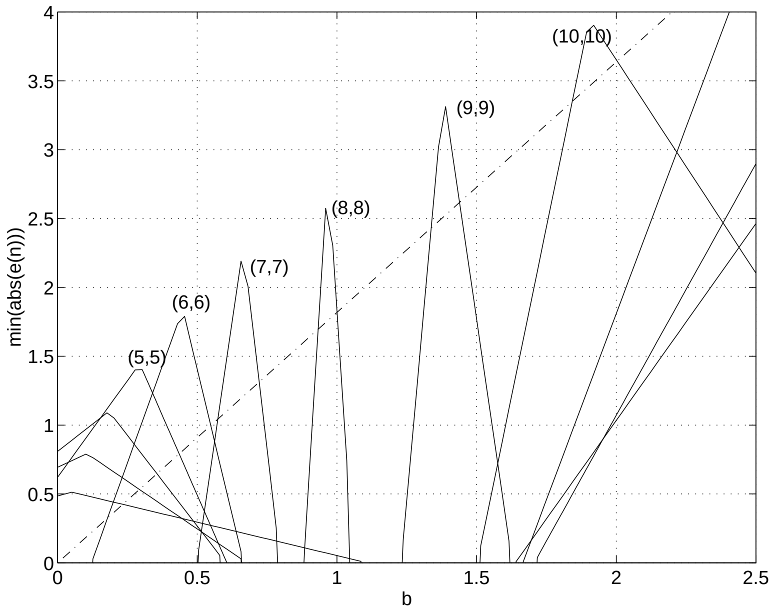

Figure 3.17: Minimum quantizer input magnitudes of a number of $(\overline{p,p})$ limit cycles for the second order modulator of Eq. (3.18) as a function of b. Magnitudes under the dashed line indicates that the corresponding limit cycle enters the noninvertible region U.

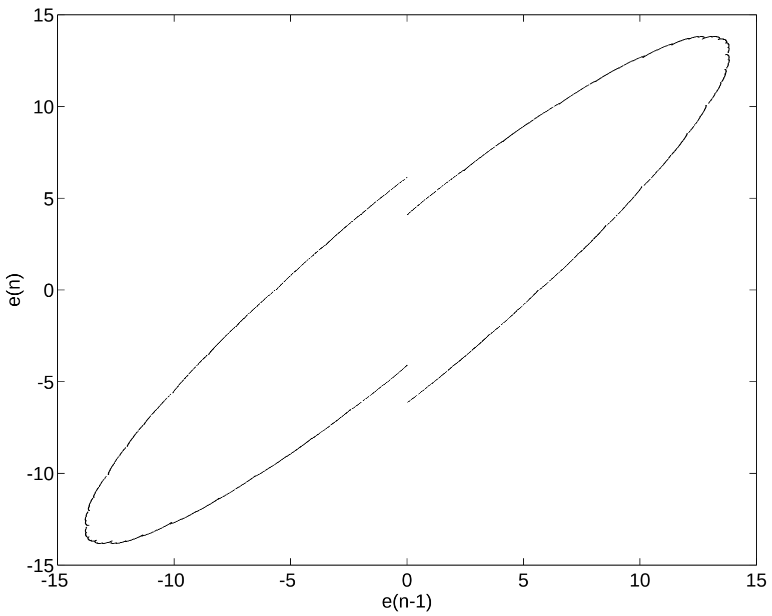

Figure 3.18: Chaotic repeller obtained by reverse time simulation for the modulator cf. Eq. (3.18) with zero input and $b = 1.1$.

also predicts the existence of a window with a chaotic repeller for b between approx. 0.75 and 0.9 which is confirmed by simulations. Later for b between approx. 1.0 and 1.3 there is another window with a chaotic repeller and for $b = 1.1$ a very interesting repeller can be observed in Fig. 3.18 using reverse time simulation. The repeller forms an almost smooth one dimensional curve with an elliptical shape. This is probably due to the fact that the $(\overline{2,2})$ limit cycle disappears for $b > 1.1$ and no $(\overline{p,p})$ limit cycles at all exist until a $(\overline{9,9})$ limit cycle appears at approx. $b = 1.25$.

For zero input and $b > 1$, two fixed points e^*_- and e^*_+ emerge. They can be located using the feedback transfer function of Eq. (3.18) evaluated at $z = 1$:

$$\begin{aligned} -\mathrm{sgn}(e^*)H(z=1) = e^* \quad &\Leftrightarrow \\ e^* = \pm\tfrac{b-1}{0.15} \quad &, b > 1 \end{aligned} \tag{3.19}$$

These fixed points are outside V and U for:

$$\begin{aligned} &\tfrac{b-1}{0.15} > \tfrac{2b}{1.1} \quad \Leftrightarrow \\ &b > 1.375 \end{aligned} \tag{3.20}$$

At $b = 1.375$ there is also a $(\overline{9,9})$ limit cycle outside U thus giving a total of three limit sets which all can be trapping in reverse time. However, simulations have shown that only for initial conditions in a small neighborhood, the fixed points can be reached in reverse time so the $(\overline{9,9})$ limit cycle will dominate the shape of B_L, i.e., the limit cycle is on ∂B_L. To be exact: the fixed points will also be on ∂B_L if they do not belong to the forward chaotic limit set L, but in that case the fixed points are fully surrounded by B_L, i.e., a deleted neighborhood of each fixed point exists which is contained in B_L. In fact simulations show that the fixed points outside U are not included in L and it seems to be a general fact that L is strictly composed of limit cycles (and fixed points) which enter U. Fig. 3.19 shows L and B_L for $b = 1.7$ where a chaotic repeller coexists with the fixed points at $e^* = \pm 0.7/0.15 = \pm 4\frac{2}{3}$ which seem to 'blow holes' in L. Between $b = 1.8$ and $b = 2$ the system has one dominant $(\overline{10,10})$ limit cycle outside U and for $b > 2$ a region with a chaotic repeller starts. When b exceeds approx. 2.1 the system becomes unstable and reverse time simulations using random branches are asymptotically trapped by the fixed points outside U after a chaotic transient □

When a forward orbit of a modulator shows long code segments which correspond to orbits on ∂B_L, it can be concluded that the forward limit set is very close to a collision with ∂B_L. The knowledge of the limit sets on ∂B_L can thus be used to give early warnings against instability.

3.8 Unreliable Modulators

The definition of the escape rate shows that instability is a matter of degrees; if γ is very small it is very unlikely that instability occurs for even long simulations. Since the computational resources limit the maximum practical length of simulations, there might exist unstable systems with very small escape rate which cannot with certainty be classified correctly as unstable by means of simulations. This is especially problematic for

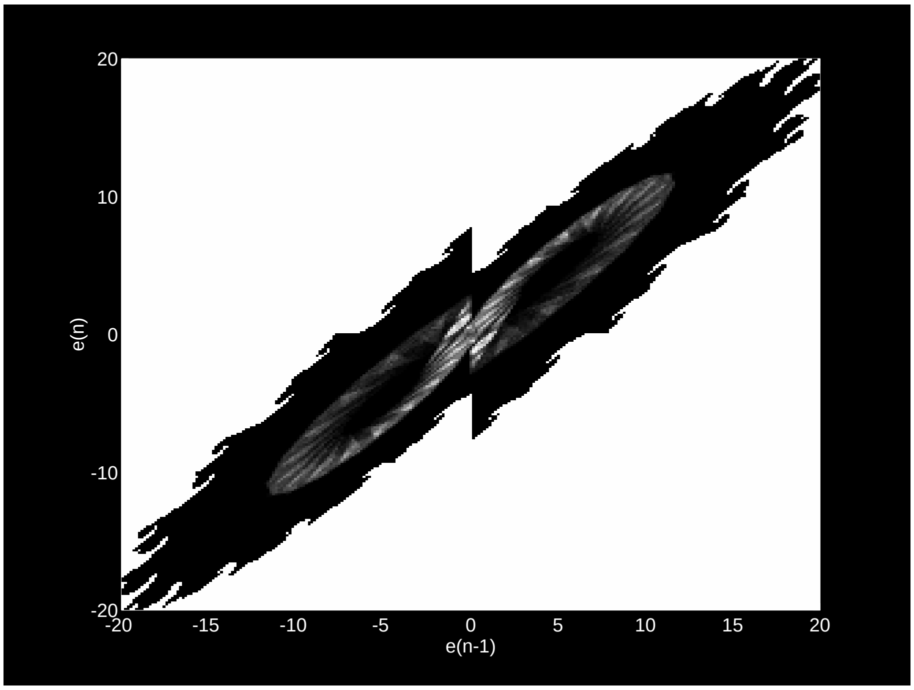

Figure 3.19: Basin of attraction and limit set for the modulator cf. Eq. (3.18) with zero input and $b = 1.7$. Notice the behavior of the limit set around the repelling fixed points at $e^* = \pm 0.7/0.15 = \pm 4\frac{2}{3}$.

systems which have an escape rate which changes slowly with parameter perturbations: if the systems show a weak instability on the longest time scale simulations allow, it is not certain that a perturbation normally improving stability, e.g., reduction of the input signal amplitude, will ensure stability. Such systems are loosely defined as being *unreliable*. On the other hand, for a *reliable* modulator the escape rate increases fast when instability occurs and stability can easily be assured by a slight perturbation in parameter space. If the perturbation is in the wrong direction, the escape rate will increase significantly and a perturbation in the opposite direction can be used.

Example 3.9 Recall the second order modulator used in Example 3.8 with feedback transfer function given in Eq. (3.18). The bifurcation diagram in Fig. 3.17 shows that a region exists for $b < 0.4$ where several $(\overline{p,p})$ limit cycles coexist outside U and several of these can be globally attracting in reverse time. In this region B_L is very complex and starts having 'holes' due to the fact that points on ∂B_L emerges at places which formerly were inside B_L.

The basin of attraction is shown in Fig. 3.20 for zero input and $b = 0.26$ and the corresponding chaotic limit set is shown of Fig. 3.21. This is very clearly an example of an unreliable modulator: the chaotic limit set is scattered about and fully surrounded by holes in B_L. A slight parameter perturbation may cause a collision between L and one of the holes in B_L resulting in a unstable system, probably with a low escape rate.

The basin of attraction forms again spirals around a limit cycle; this time the $(\overline{5,5})$ limit cycle which as expected is outside U. At the same time the

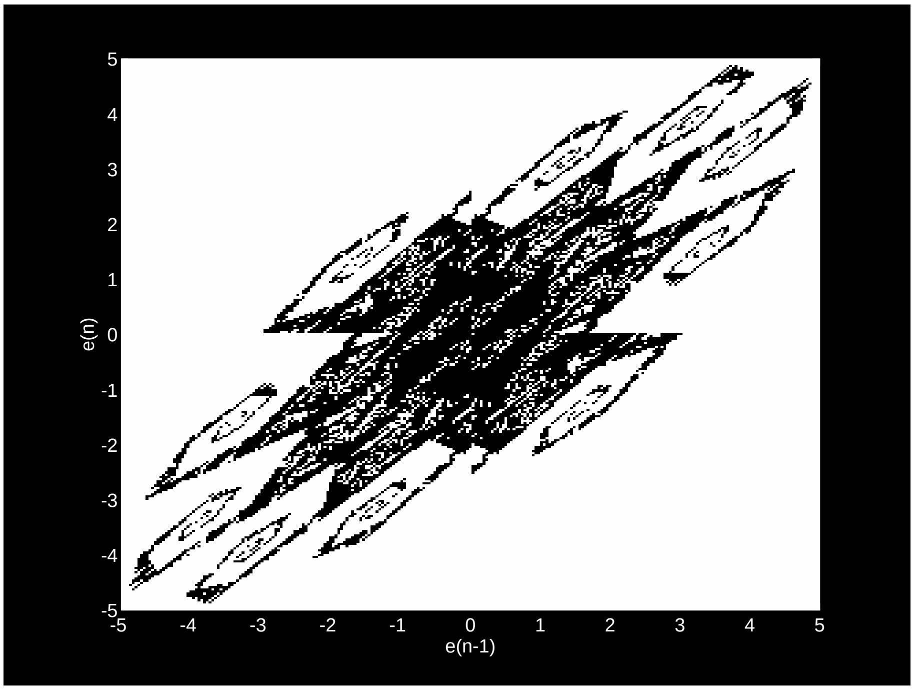

Figure 3.20: Basin of attraction for the modulator cf. Eq. (3.18) with zero input and $b = 0.26$.

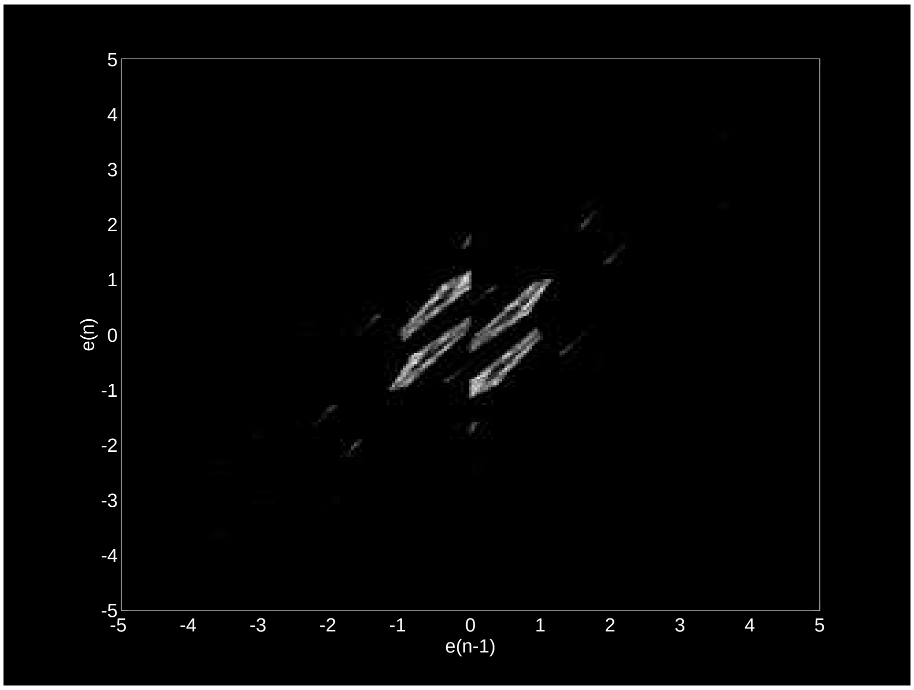

Figure 3.21: Limit set for the modulator cf. Eq. (3.18) with zero input and $b = 0.26$.

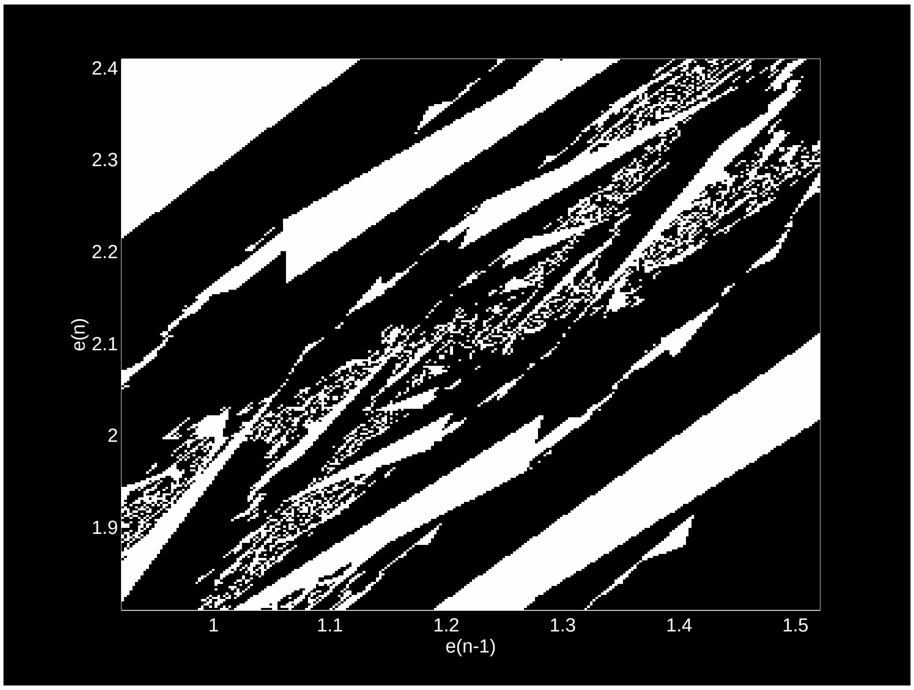

Figure 3.22: Magnified plot of the basin of attraction for the modulator cf. Eq. (3.18) with zero input and $b = 0.26$. The center of the plot is a point on the $(\overline{4,4})$ limit cycle.

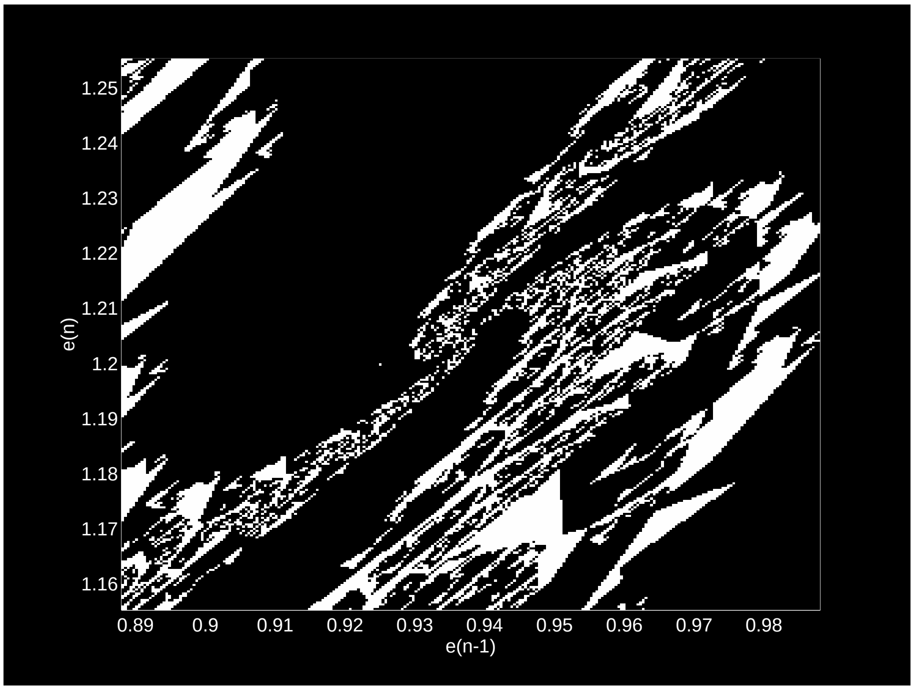

Figure 3.23: Magnified plot of the basin of attraction for the modulator cf. Eq. (3.18) with zero input and $b = 0.26$. The center of the plot is a point on the $(\overline{3,3})$ limit cycle.

limit cycles $(\overline{6,6})$, $(\overline{4,4})$ and $(\overline{3,3})$ exist and all of them are outside U as well. However, the $(\overline{5,5})$ limit cycle has the highest minimum quantizer input magnitude. A closer inspection of the magnified plots in Fig. 3.22 and Fig. 3.23 reveals that B_L also forms internal spirals around the $(\overline{4,4})$ and $(\overline{3,3})$ limit cycles and these internal spirals can explain the holes in B_L. The $(\overline{6,6})$ limit cycle is totally outside B_L indicating that this limit cycle can only be reached in reverse time from outside B_L. The strange B_L set can thus be explained by the coexistence of several limit cycles on ∂B_L outside U which all are globally attracting in a reverse time simulation using random branches □

The previous example showed clearly that stability analysis of second-order modulators is generally very complicated. The next example validates a stability criterion derived in Example 3.4 for a certain class of second-order modulators.

Example 3.10 The stability of a certain class of second-order modulators with a real pole outside and inside the unit circle was investigated in Example 3.4. It was possible to derive a sufficient stability criterion (Eq. (3.15) and Eq. (3.17). In order to validate the analysis, the parameter space (b, i) was investigated by simulations for $a = -0.05$, i.e., b and i was sampled in a uniform 512×512 grid for $0 < b < 1.5$ and $0 < i < 1$. For each point, the modulator was simulated 200 times with random initial conditions. The simulations was stopped when the stable manifolds were crossed (i.e., when the system escaped) or when a maximum of 1000 iterations was elapsed. For each parameter set, the average iteration number was determined and the result is shown in Fig. 3.24 using a gray scale. The criteria of Eq. (3.15) and Eq. (3.17) are shown as black curves. Eq. (3.15) is very accurate and the onset of stability for $\sqrt{b} < -a$ is very sudden. For $\sqrt{b} > -a$, the Eq. (3.17) criterion is very conservative and the onset of instability is not so well defined. This is clearly a more unreliable region. For b approaching unity, the plot is rippling for increasing input i, i.e., there are unstable 'ridges' with stable 'valleys' in between. When a valley is followed, the mean survival time is only increasing slowly □

3.9 Nonchaotic Modulators

When the modulator is nonchaotic, allmost all limit cycles are attracting, i.e., asymptotically stable [25]. This means that after a transient the modulator will asymptotically end on a limit cycle, regardless of the initial condition. Consequently, the basins of attraction corresponding to all the limit cycles will induce a partitioning on the entire state-space. The basin boundaries can be very complex and this gives rise to very long chaotic transients before the orbit is attracted to a limit cycle.

For high-order modulators ($N > 2$), some of the limit cycles may have extreme magnitudes and give poor signal-to-noise ratios. Consequently, when a modulator is attracted to such a limit cycle, the modulator is practically unstable. Normally, it is easy to distinguish limit cycles corresponding to stable and unstable modulator operation since limit cycles with unstable operation have extreme maximum amplitudes. The state-space can thus

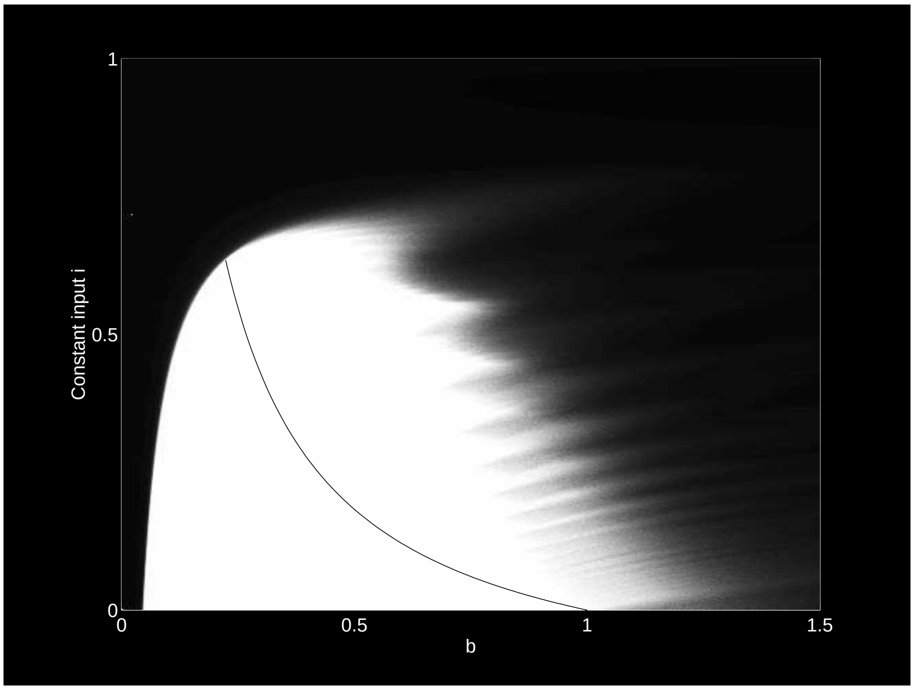

Figure 3.24: A gray-scale plot of the mean survival time of the modulator of Example 3.4 with $a = -0.05$. The white region has a mean survival time of a minimum of 1000 time-steps. Darker regions have lower survival time.

naturally be partitioned into two disjoint sets B_S and B_U, i.e., sets of points which are attracted to 'stable' and 'unstable' limit cycles, respectively. This fact emphasizes that the practical modulator stability concept must not be confused with the asymptotical stability of limit sets, cf. Definition 2.3. In fact, it is very difficult to give an adequate and comprehensive stability definition for nonchaotic modulators. This question will be discussed later in chapter 5.

3.10 Summary

This chapter analyzed basins of attraction of chaotic modulators. The onset of instability was characterized as a boundary crisis, i.e., the chaotic limit set collides with the boundary of the basin of attraction. After the collision, the chaotic attractor becomes an unstable repeller. The degree of instability was quantified through the definition of the escape-rate which is the slope of the survival probability versus iteration number in lin-log plot. There is always a positive probability that the system survives for arbitrarily long time; the closer the initial condition is on the repeller, the longer the system survives.

Some first and second-order systems were investigated in detail. The different examples showed the complexity of the basin of attraction for chaotic second-order systems. In some cases, a chaotic repeller is found on the boundary of the basin of attraction. The parameter regions for which a boundary repeller existed could be predicted using limit cycle analysis.

The complexity of even second-order modulators shows how difficult it is to derive a comprehensive, general and not to conservative stability criterion. Only in a few special cases of second-order modulators, it has been possible to derive analytical stability criteria.

It was shown that the onset of instability can occur very differently: for some systems, the escape rate only increases slowly for varying parameters. Such systems were called unreliable because the existence of parameter regions with very low but positive escape rate makes instability very difficult to detect using simulations.